catalysts

MDPI

Review

Research Progress on Zeolite-Type High-Temperature NH_3-SCR Catalysts

Xuewen Mu [1,2], Xue Bian [1,2,*], Yuting Bai [3], Meng Zha [1,2], Yu Huang [1,2] and Jing Wei [1,2]

[1] Key Laboratory of Ecological Metallurgy of Multi-Metal Intergrown Ores of Ministry of Education, Shenyang 110819, China; muxuewen000115@163.com (X.M.); zhameng010518@163.com (M.Z.); huangyv2000@163.com (Y.H.); weifs107@163.com (J.W.)
[2] School of Metallurgy, Northeastern University, Shenyang 110819, China
[3] School of Metallurgy and Materials Engineering, Liaoning Institute of Science and Technology, Benxi 117004, China; baiyuting0220@163.com
* Correspondence: bianx@smm.neu.edu.cn

Abstract

Gas turbines operate at exhaust gas temperatures exceeding 500 °C. Vanadium-based catalysts encounter challenges in NH_3-SCR denitrification due to vanadium volatilization and titanium dioxide support phase transition at high temperatures. This restricts the effective denitrification temperature range to 300~400 °C, falling short of gas turbine denitrification requirements. Zeolite-supported catalysts, known for their high specific surface area, abundant acid sites, and stable framework structure, demonstrate superior catalytic activity and hydrothermal stability at high temperatures. This review synthesizes recent advancements in high-temperature catalysts utilizing ZSM-5, Beta, SSZ-13, and SAPO-34 zeolites as supports. It elucidates the interaction mechanisms between active components (e.g., transition metals Fe, Cu, W, rare earth elements) and zeolite supports. Furthermore, it examines variations in denitrification performance through the lens of the high-temperature NH_3-SCR reaction mechanism, offering valuable insights for high-temperature denitrification catalyst development.

Keywords: gas turbines; NH_3-SCR; high-temperature denitrification; zeolite catalysts; reaction mechanism

check for updates

Academic Editors: Guido Busca and Narendra Kumar

Received: 13 September 2025
Revised: 3 October 2025
Accepted: 4 November 2025
Published: 6 November 2025

Citation: Mu, X.; Bian, X.; Bai, Y.; Zha, M.; Huang, Y.; Wei, J. Research Progress on Zeolite-Type High-Temperature NH_3-SCR Catalysts. *Catalysts* **2025**, *15*, 1060. https://doi.org/10.3390/catal15111060

Copyright: © 2025 by the authors. Licensee MDPI, Basel, Switzerland. This article is an open access article distributed under the terms and conditions of the Creative Commons Attribution (CC BY) license (https://creativecommons.org/licenses/by/4.0/).

1. Introduction

As a core flexible power generation technology supporting the integration of high proportions of renewable energy, gas turbines play a key role in the global energy transition [1–3]. However, their high-temperature exhaust gases (typically > 500 °C) make nitrogen oxide (NO_x) emissions reduction a major bottleneck constraining their compliant operation [4]. Unlike traditional coal-fired flue gas, gas turbine flue gas has extremely low particulate matter and SO_2 content [5,6], enabling its denitrification system to adopt a simpler, lower-cost high-temperature configuration without needing to address traditional challenges such as catalyst blockage and ammonium bisulfate poisoning [7,8]. However, this high-temperature advantage imposes extremely stringent requirements on the denitrification catalyst itself. Commercially available V_2O_5-$WO_3(MoO_3)/TiO_2$ catalysts rapidly deactivate at temperatures exceeding 500 °C due to issues such as the volatilization of the active component vanadium, crystal structure transformation of the TiO_2 support, and particle sintering, making them unsuitable for direct application [9–14]. Based on actual operating data from gas turbines, flue gas temperatures typically fluctuate between

500~650 °C (reaching up to 680 °C under variable load conditions) [15–19], while commercial vanadium-based catalysts cannot operate stably above 500 °C [20,21]. Therefore, developing a highly efficient and stable NO_x reduction catalyst covering the 500~650 °C temperature window is critical to achieving deep NO_x purification in gas turbines.

To address this challenge, researchers have extensively explored various metal oxide catalysts. For instance, Zhang et al. [22] introduced Co oxide-modified vanadium-based catalysts, leveraging their enhanced surface acidity and redox capabilities to achieve over 90% NO_x conversion rates within the 300~550 °C range. The W-Zr-O_x/TiO_2 catalyst developed by Chen et al. [23] formed solid hyperacid sites on the TiO_2 surface, increasing acid and oxygen vacancy concentrations to maintain high activity between 330~600 °C. Leveraging CeO_2's superior oxygen storage capacity, our group developed a Ce-W/Ti-Si catalyst exhibiting over 80% NO conversion efficiency across 225~560 °C [24]. Although the aforementioned strategies of modifying active components to optimize acidity and redox capabilities demonstrate significant effectiveness in the high-temperature range, none have overcome the inherent structural defect of metal oxide catalyst systems—insufficient thermodynamic stability of the support [25–27]. Whether TiO_2, Al_2O_3, or other common metal oxide supports, severe sintering and phase transformations occur above 600 °C. This structural collapse of the support leads to a drastic decrease in specific surface area, pore blockage, and agglomeration and deactivation of the loaded active components [28]. Therefore, although modifying the active component can optimize catalytic performance to some extent [29–32], the thermal stability of the support itself fundamentally limits the upper temperature limit of the entire catalyst system, preventing it from meeting the stable operating requirements of the 500~650 °C full operating window in gas turbines.

Given the inherent limitations of metal oxide supports, research focus inevitably shifts toward thermally stable zeolite materials [33–35]. Unlike amorphous or semi-crystalline supports such as TiO_2, the crystalline framework of zeolites (e.g., the MFI structure in ZSM-5) exhibits exceptional thermal stability, withstanding temperatures exceeding 800 °C [36]. This fundamentally resolves core challenges associated with support sintering and phase transitions. Simultaneously, their vast specific surface area (300~1000 m^2/g) and well-ordered pore systems not only effectively stabilize and disperse metal active sites while inhibiting sintering but also optimize mass transfer efficiency for reactant molecules [37]. In recent years, zeolite catalysts loaded with active sites such as Cu, Fe, Ce, and W (e.g., ZSM-5 [38,39], Beta [40,41], SSZ-13 [42–44], SAPO-34 [45,46]) have emerged as a frontier research direction in high-temperature denitrification. However, significant bottlenecks persist in this field: First, the structure-activity relationships between different active components (single-metal/multi-metal) and various zeolite supports remain unclear [47–49]. Second, research on reaction mechanisms and deactivation mechanisms in the ultra-high-temperature zone above 600 °C remains relatively weak [50,51]. Furthermore, existing studies predominantly focus on performance optimization at the laboratory scale, lacking systematic evaluation of the large-scale production costs, hydrothermal stability, and lifecycle of zeolites with diverse structures. This severely limits their industrial applicability [52]. The ambiguity surrounding these critical scientific issues significantly hinders the rational design and development of next-generation high-temperature catalysts for gas turbine applications.

Several reviews have explored NH_3-SCR catalysts, including zeolite-based systems [53–55]. However, most studies have focused on low-temperature applications, single zeolite types, or fundamental theories. This has resulted in a gap in systematic analysis and comparison of multiple zeolite frameworks under high-temperature conditions (>500 °C), particularly lacking in-depth exploration of the interactions between framework stability, active site engineering, and industrial feasibility.

This review aims to fill this gap by critically synthesizing research advances in zeolite-based high-temperature NH_3-SCR catalysts from 2018 to 2025. We focus on extensively studied and promising supports—ZSM-5, Beta, SSZ-13, and SAPO-34—while exploring emerging materials such as SSZ-16 (AFX). This paper systematically analyzes advances in single-metal (Cu, Fe) and composite metal-modified zeolite catalysts. Unlike previous studies, we emphasize: (1) elucidating structure-activity relationships and reaction mechanisms specific to high-temperature operating conditions; (2) critically evaluating performance trade-offs related to framework topology, hydrothermal stability, and synthesis costs; (3) Providing forward-looking perspectives on challenges and opportunities for commercial application through discussions integrating advanced characterization, machine learning-assisted design, and green synthesis routes. This paper aims to offer comprehensive references and valuable insights for researchers engaged in the rational design and development of next-generation high-temperature denitration catalysts for gas turbines.

2. Structural and Functional Comparison of Zeolite Support

The selection of zeolite supports in high-temperature "NH_3-Selective Catalytic Reduction (NH_3-SCR)" denitrification technology is fundamentally determined by their combined structural and chemical properties, which directly govern the catalyst's catalytic activity and durability [56]. Unlike traditional V_2O_5-WO_3(MoO_3)/TiO_2 catalysts constrained by thermal stability [57], zeolite-based catalyst systems enable tunable architectural design through framework topology, pore geometry, and acidic site engineering [58]. Table 1 summarizes the structural parameters of zeolites with different topologies [59].

Table 1. Structural parameters of the zeolites with different topologies [59].

Topology	Name	Maximum Diameter (Å)	Channel System	Ring Member	Synthesis Cost	Hydrothermal Stability
MFI	ZSM-5	5.1 × 5.5 5.3 × 5.6	3-dimensional	10/6/5/4	Medium	Low
BEA	Beta	6.6 × 6.7 5.6 × 5.6	3-dimensional	12/6/5/4	Medium	Medium
CHA	SSZ-13 SSZ-62 SAPO-34 SAPO-47	3.8 × 3.8	3-dimensional	8/6/4	High	Excellent
AFX	SSZ-16 SAPO-56	3.4 × 3.6	3-dimensional	8/6/4	High	Excellent
AEI	SSZ-39 SAPO-18	3.8 × 3.8	3-dimensional	8/6/4	High	Excellent
LTA	UZM-9 SAPO-42	4.1 × 4.1	3-dimensional	8/6/4	High	Good

MFI zeolites (represented by ZSM-5) find extensive applications in catalysis, adsorption, and separation due to their three-dimensional cross-linked pore structure and tunable acidity [60,61]. However, their poor hydrothermal stability and high-temperature metal agglomeration issues limit their use under harsh conditions [62]. BEA-type zeolites (represented by Beta) exhibit outstanding mass transfer capabilities due to their three-dimensional 12-membered ring macroporous structure and high specific surface area. However, their complex structure (highly defective, two polymorphic structures) adversely affects hydrothermal stability [63]. CHA-type zeolites (e.g., SSZ-13, SAPO-34)

exhibit outstanding hydrothermal stability and good catalytic performance due to their cage-like topology [64–66]. However, their widespread application is constrained by the high cost of template agents (e.g., *N*,*N*,*N*-trimethyl-1-adamantammonium hydroxide) and complex synthesis processes [67–69]. The three-dimensional octahedral ring dual-channel system of AFX-type zeolites (such as SSZ-16) effectively balances the diffusion and selectivity of small molecules [70]. However, the high cost of template agents (such as amantadine derivatives) and potential channel blockage issues severely hinder their large-scale practical application [71,72]. AEI zeolites (e.g., SSZ-39) exhibit outstanding catalytic performance due to their unique three-dimensional channels [73], yet high synthesis costs (*N*,*N*-dimethylpiperidinium templates) similarly restrict their adoption [74]. LTA zeolites (e.g., 4A) remain irreplaceable in small-molecule sieving and ion exchange [37], but their narrow octahedral ring window and low thermal stability limit catalytic functionality [75].

The comparative analysis above indicates that no single zeolite support excels in all aspects. These performance differences fundamentally stem from the unique framework constraints of each support and the synergistic interaction between the active components and the support [76,77]. Based on this, the following section will delve into modification strategies for various zeolite supports (ZSM-5, Beta, SSZ-13, SAPO-34, etc.). It summarizes the interactions between active components—such as transition metals (Fe, Cu, W) and rare earth elements—and different support types, while exploring their NH_3-SCR reaction mechanisms. This analysis aims to provide insights for developing high-temperature denitrification catalysts.

3. ZSM-5 Support

Among various zeolite supports, ZSM-5 (MFI topology) has garnered significant attention due to its unique pore structure, strong acidity, high specific surface area, and excellent thermal stability [37]. Its relatively simple synthesis process and low cost further position it as a commercially promising SCR catalyst support. This section critically reviews research progress on single-metal and multi-metal modified ZSM-5 catalysts, focusing on design principles, catalytic performance, and reaction mechanisms under high-temperature conditions.

3.1. Single Metal-Doped ZSM-5 Catalyst

Among various metal-modified ZSM-5 catalysts, Fe is the most extensively studied and effective active metal in high-temperature NH_3-SCR systems due to its excellent redox properties and ability to form highly active sites [38,39,78–87].

Fe/ZSM-5 catalysts represent one of the earliest zeolite-type denitrification catalysts studied. Long and Ma et al. [78,79] reported nearly simultaneously in 1999 that Fe/ZSM-5 catalysts exhibit high NH_3-SCR reaction activity. Long found that Fe/ZSM-5 catalysts achieve nearly 100% NO conversion within the 400~550 °C temperature range (Figure 1). Subsequently, Long et al. [80] conducted detailed studies on the NH_3-SCR reaction mechanism of Fe/ZSM-5 catalysts. They proposed that the NH_3-SCR reaction on Fe/ZSM-5 catalysts follows the "Eley-Rideal (E-R)" reaction model (Figure 2). In the gas phase, NH_3 molecules adsorb and activate at Brønsted acid sites to form NH_4^+, while NO molecules oxidize on Fe^{3+} to form NO_2. Subsequently, adsorbed NH_3 reacts with gas-phase NO_2 to generate the intermediate NO_2 $[NH_4^+]_2$, which then reacts with gas-phase NO to yield the final products N_2 and H_2O.

The silica–alumina ratio of different zeolites and the preparation method of catalysts significantly influence NH_3-SCR activity. Brandenberger et al. [81] used NH_4-ZSM-5 zeolite with a Si/Al ratio of 14 as a support and found that Fe/ZSM-5 catalysts prepared via liquid ion exchange exhibited NO conversion rates exceeding 80% within the 350~650 °C range.

Qi et al. [82] investigated the effects of SiO_2/Al_2O_3 ratios (11, 25, 40) and iron sources ($FeCl_2$ and $FeCl_3$) on catalyst performance. They demonstrated that catalysts prepared using $FeCl_2$ as the active component exhibited higher activity than those using $FeCl_3$. When $FeCl_2$ was the iron source, the Fe/ZSM-5 catalyst exhibited optimal activity at a Si/Al ratio of 11 and an iron loading of 2.5 wt%, achieving NO conversion rates exceeding 80% between 320~550 °C. The study revealed that SCR activity decreases with increasing Si/Al ratio in the ZSM-5 support. This is attributed to the higher Brønsted acidity of ZSM-5 zeolites with lower Si/Al ratios. Strong acidity promotes NH_3 adsorption, thereby enhancing the activity of Fe/ZSM-5 catalysts.

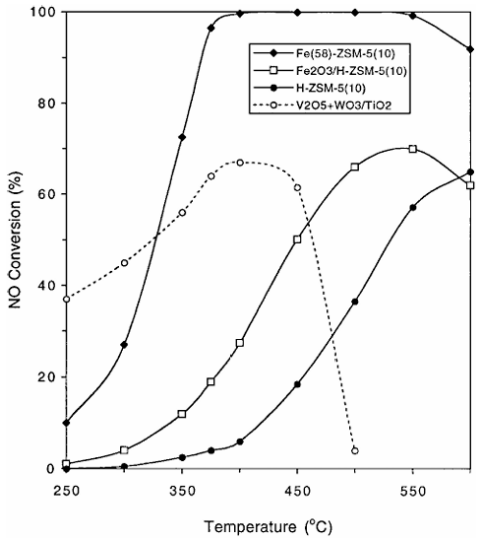

Figure 1. Catalytic activities for SCR of NO by ammonia on H/ZSM-5, Fe_2O_3-H/ZSM-5, Fe/ZSM-5, and V_2O_5-WO_3/TiO_2 catalysts. Reaction conditions: [NO] = [NH_3] = 1000 ppm, [O_2] = 2%, He balance, GHSV = 460,000 h^{-1} [78].

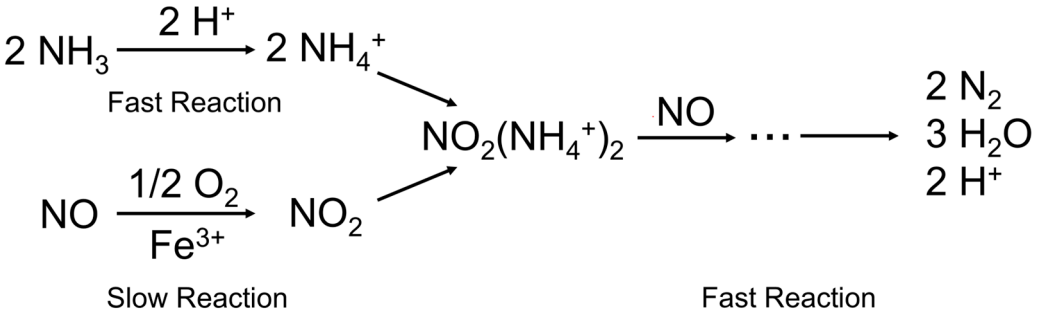

Figure 2. Reaction scheme of SCR of NO with ammonia on Fe/ZSM-5 [80].

Regarding catalyst preparation methods, Shi et al. [83,84] investigated the effects of liquid ion exchange, solid ion exchange, and isovolumetric impregnation on the denitrification performance and mechanism of Fe/ZSM-5 catalysts. The study revealed that Fe/ZSM-5 catalysts prepared via isovolumetric impregnation exhibited optimal denitrification activity, achieving a maximum NO_x conversion rate of 100% and maintaining over 90% conversion efficiency even at 550 °C. Wang et al. [38,39] investigated the effects of equal-volume impregnation and aqueous solution ion exchange on the NO_x removal performance of Fe/ZSM-5 catalysts. Results indicated that the Fe/ZSM-5 catalyst with 1.0 wt% Fe content prepared by equal-volume impregnation exhibited NO_x conversion rates exceeding 80% between 425~680 °C (Figure 3a). At elevated temperatures, this catalyst exhibits enhanced strength of strong acidic sites with decreasing Fe loading (Figure 3b) and reduced non-selective oxidation of NH_3 (Figure 3c), thereby demonstrating excellent

high-temperature NO_x removal performance. DRIFT testing confirmed the coexistence of "Langmuir-Hinshelwood (L-H)" and E-R reaction pathways. However, DRIFT results reveal that for Fe/ZSM-5 catalysts prepared via aqueous solution ion exchange, the primary SCR reaction pathway is the E-R mechanism. This arises from the reaction mechanism between adsorbed NO and gaseous NH_3, as depicted in Equations (1)–(3) and Figure 4 (where S represents the zeolite structure) [39]. This indicates that the reaction mechanism of the Fe/ZSM-5 catalyst is closely related to its preparation method.

$$[S - Fe^{3+} = O] + NO \rightarrow [S - Fe^{3+} = O][NO] \quad (1)$$

$$[S - Fe^{3+} = O][NO] + NH_3 \rightarrow N_2 + H_2O + [S - Fe^{2+} - OH] \quad (2)$$

$$[S - Fe^{2+} - OH] + 1/4\ O_2 \rightarrow 1/2\ H_2O + [S - Fe^{3+} = O] \quad (3)$$

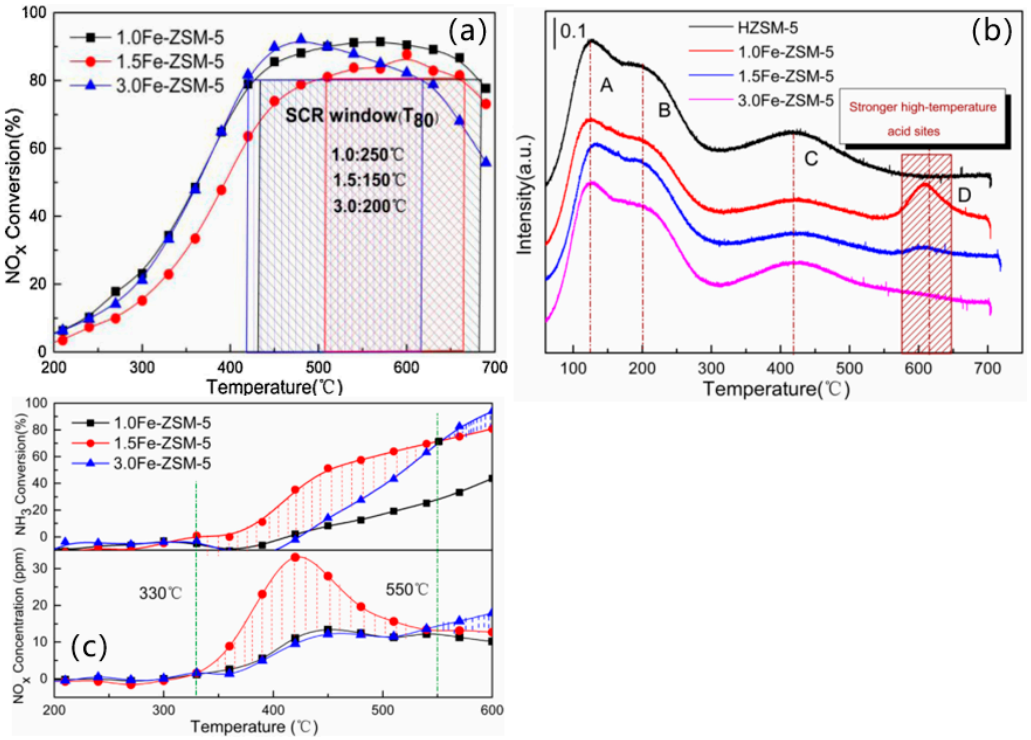

Figure 3. (**a**) Catalytic activity of the Fe/ZSM-5 catalyst; (**b**) Profiles of NH_3-TPD measurements over the Fe/ZSM-5 catalysts with 1.0, 1.5 and 3.0 wt% Fe content; (**c**) NO concentration and NH_3 conversion during the NH_3 oxidation over the Fe/ZSM-5 catalysts. Reaction conditions: [NO] = [NH_3] = 500 ppm, [O_2] = 8%, [CO_2] = 5%, N_2 balance, GHSV = 50,000 h^{-1} [38].

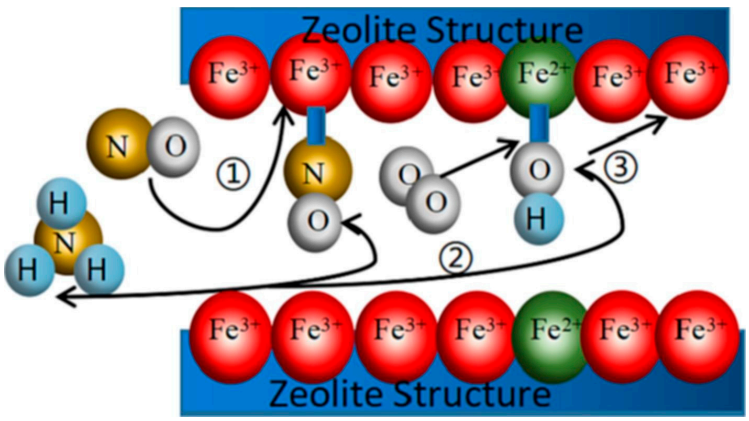

Figure 4. The main SCR reaction mechanism for the Fe/ZSM-5 zeolite [39].

3.2. Composite Metal-Doped ZSM-5 Catalyst

To further enhance high-temperature activity and hydrothermal stability, introducing a second or third metal to generate synergistic effects has proven to be a highly effective strategy, typically yielding superior performance compared to single-metal catalysts.

CeO_2 possesses high oxygen storage and redox capacity. As an active component, it can synergistically interact with other transition metals to enhance the catalyst's denitrification performance. Chen et al. [85] investigated Ce- or La-modified Fe/ZSM-5 catalysts, finding that Ce-modified Fe/ZSM-5 exhibits a broader active temperature window. Long et al. [86] observed that Ce-Fe/ZSM-5 catalysts prepared via ion exchange achieved NO conversion rates exceeding 90% within the 370~600 °C range. Wang et al. [87] employed $Fe(NO_3)_3{\cdot}9H_2O$, $Ce(NO_3)_3{\cdot}6H_2O$, and ZSM-5 zeolite (SiO_2/Al_2O_3 = 27) as raw materials to prepare a series of Ce-Fe/ZSM-5 catalysts via an isovolumetric impregnation method. Their study revealed that Fe_4/ZSM-5 catalysts with 4 wt% Fe exhibited severe ammonia oxidation at high temperatures. However, loading a certain amount of Ce increased the strength and quantity of surface acids, particularly Lewis acid sites, thereby reducing the proportion of adsorbed oxygen on the surface. exhibited severe ammonia oxidation at elevated temperatures. Loading Ce increased both the strength and quantity of surface acids, particularly Lewis acid sites, while enhancing the proportion of adsorbed oxygen. The synergistic interaction between Ce and Fe improved the catalyst's high-temperature redox capacity, suppressing NH_3 oxidation to NO and boosting high-temperature activity. At 550 °C, the NO_x conversion rate of the Fe_4/ZSM-5 catalyst was only 77.11%. When Ce was loaded at 1 wt%, the Ce_1-Fe_4/ZSM-5 catalyst achieved a NO_x conversion rate exceeding 95% across the 400~550 °C range. After hydrothermal aging, the NO_x conversion rate remained approximately 90% within the 450~550 °C range, demonstrating good hydrothermal stability.

WO_3 is an excellent solid acid commonly used as an active component in SCR applications. ZrO_2 is an acid-base amphoteric oxide with favorable redox properties. Consequently, some researchers have employed both WO_3 and ZrO_2 as active components to enhance the NH_3-SCR performance of catalysts. Chen et al. [23] discovered that WO_3 and ZrO_2 form a solid hyperacid (W-Zr-O_x). The interaction between WO_3 and ZrO_2 significantly enhances the catalyst's surface acidity and redox properties, thereby effectively improving its high-temperature activity. Feng et al. [88] investigated the effects of three preparation methods—sol–gel, impregnation, and grinding—on W-Zr/ZSM-5 catalyst performance using ZSM-5 as a support. Results indicated that the sol–gel-prepared catalyst exhibited optimal activity. attributed to greater surface enrichment of W and Zr elements. This promotes the formation of acidic sites on the catalyst surface, while the interaction between WO_3 and ZrO_2 creates oxygen vacancies (Figure 5), enhancing the catalyst's redox properties. After calcination at 700 °C for 2 h, the W-Zr/ZSM-5 catalyst (15 wt% WO_3 and 1 wt% ZrO_2) exhibited NO conversion rates exceeding 90% within the 350~630 °C range. In situ infrared studies revealed that NO removal on the W-Zr/ZSM-5 catalyst follows the L-H reaction mechanism, with amide species (-NH_2), monodentate nitrite, NH_4^+, surface-adsorbed NH_3 species, and ad-NO_2 species were identified as key reaction intermediates at elevated temperatures. Specifically, -NH_2 and adsorbed NH_3 reacted with ad-NO_2 and ad-NO to form N_2 and H_2O, respectively. NH_4^+ reacted with ad-NO_2 to produce NH_4NO_2, which ultimately decomposed into N_2 and H_2O. Additionally, the ad-NO_2 species participates in the "rapid SCR" reaction, effectively promoting the reaction process. The reaction mechanism of the catalyst at high temperatures is shown in Equations (4)–(13).

$$NH_3(g) \rightarrow NH_4^+(a)\ (\text{Brønsted acid sites}) \quad (4)$$

$$O_2 + 2^* \rightarrow 2 - O^* \quad (5)$$

$$NH_3(g) + * \rightarrow -NH_3^* \quad (6)$$

$$-NH_3^* + -O^* \rightarrow -NH_2^* + -OH^* \quad (7)$$

$$NO(g) + -O^* \rightarrow -NO_2^* \quad (8)$$

$$NO(g) + * \rightarrow -NO^* \quad (9)$$

$$-NH_2^* + -NO_2^* \rightarrow N_2 + H_2O + -O^* \quad (10)$$

$$-NH_3^* + -NO^* \rightarrow N_2 + H_2O + -H^* \quad (11)$$

$$NH_4^+ + -NO_2^* \rightarrow NH_4NO_2 \rightarrow N_2 + 2H_2O \quad (12)$$

$$2\text{-}NH_3^* + -NO_2^* + -NO^* \rightarrow 2N_2 + 3H_2O \quad (13)$$

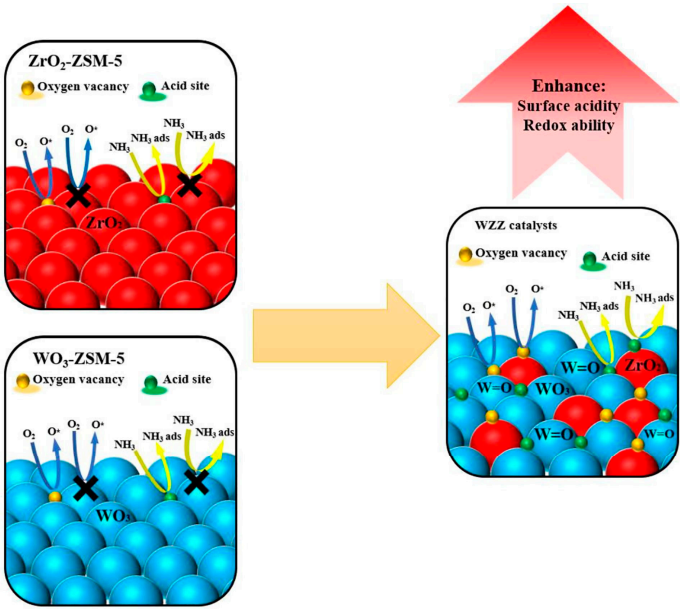

Figure 5. The schematic diagram of interaction between WO_3 and ZrO_2 [88].

Due to the excellent NO conversion rate of W-Zr/ZSM-5 catalysts at high temperatures and the ability of rare earth element doping to enhance SCR activity, Feng et al. [89] prepared Sm-W-Zr/ZSM-5 catalysts using the sol–gel method. Results indicate that the W-Zr/ZSM-5 catalyst loaded with 1.0 wt% Sm achieves complete NO conversion within the 400~600 °C range and maintains NO conversion rates exceeding 90% between 380~640 °C (Figure 6). The introduction of Sm species suppressed agglomeration of the active components (as indicated by the red arrows in Figure 7), thereby promoting dispersion of the active components on the catalyst surface and slightly improving the NH_3-SCR performance at high temperatures. Furthermore, the Sm-W-Zr/ZSM-5 catalyst exhibited excellent regeneration capability and could be regenerated through heat treatment at 350 °C.

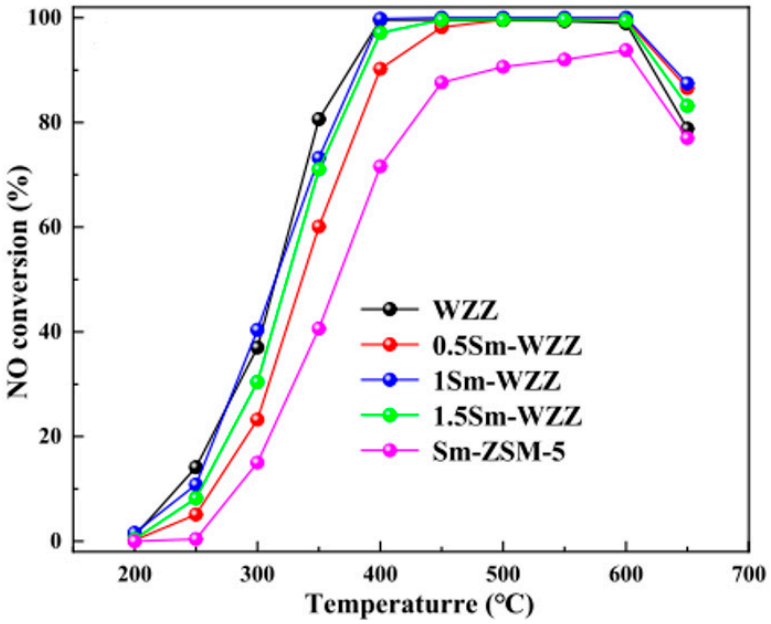

Figure 6. NO conversion of WZZ and xSm-WZZ catalysts. Reaction conditions: [NO] = [NH_3] = 500 ppm, [O_2] = 5%, N_2 balance, GHSV = 15,000 h^{-1} [89].

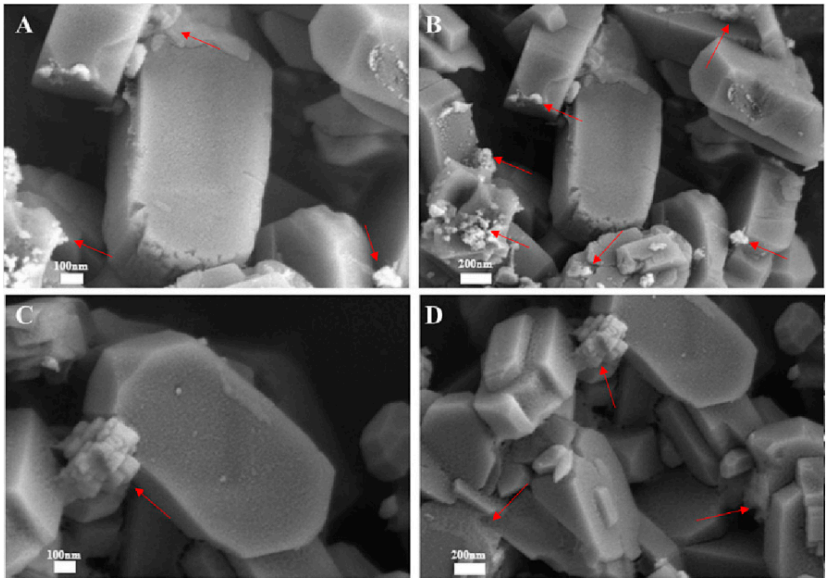

Figure 7. SEM results of WZZ (**A**,**B**) and 1Sm-WZZ (**C**,**D**) [89].

Another critical factor affecting catalyst activity at high temperatures is the overoxidation of NH_3. Liu et al. [90] discovered that the ion-exchange-prepared Fe-Ni-W/ZSM-5 ternary metal catalyst possesses Brønsted acid sites and extra-framework metal exchange sites. These active sites exhibit high activation barriers for the $NH_2 \rightarrow NH$ conversion during NH_3 oxidation, significantly suppressing NH_3 overoxidation and thereby improving high-temperature NH_3-SCR performance. Simultaneously, metal loading significantly influenced SCR performance (Figure 8a), with the catalyst containing 0.5 wt% Fe, 0.5 wt% Ni, and 0.25 wt% W exhibiting optimal activity, achieving 90% NO_x conversion efficiency between 480~750 °C. After hydrothermal aging at 800 °C, the NO conversion rate slightly decreased (Figure 8b). In situ DRIFT results revealed potential pathways for NH_3 oxidation. Initially, hydrogen is extracted from NH_3 adsorbed on the catalyst surface. As temperature increases, the reduced binding energy of metal-oxygen bonds facilitates gradual dehydro-

genation induced by active lattice oxygen in the metal oxide. Subsequently, oxidation products form in the presence of lattice/gas-phase oxygen, as depicted by Reactions (14)–(19).

$$NH_3 \rightarrow -NH_2 + *H \quad (14)$$

$$-NH_2 + O \rightarrow -NH + OH \quad (15)$$

$$-NH + O \rightarrow -N + OH \quad (16)$$

$$-NH + O \rightarrow HNO \rightarrow *H + NO \quad (17)$$

$$-N + O \rightarrow NO \quad (18)$$

$$-N + NO \rightarrow N_2O \quad (19)$$

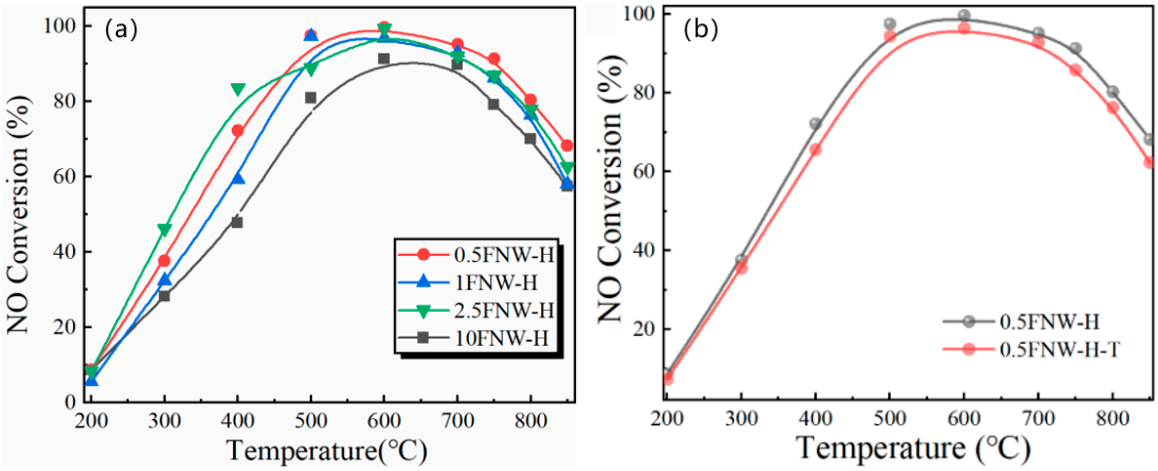

Figure 8. (**a**) Effect of metal contents over Fe-, Ni- and W-exchanged zeolite catalyst; (**b**) Effect of hydrothermal aging on 0.5FNW-H catalyst. Reaction conditions: [NO] = [NH_3] = 500 ppm, [O_2] = 6%, [H_2O] = 5.1%, N_2 balance, GHSV = 30,000 h^{-1} [90].

In summary, for high-temperature NH_3-SCR applications, ZSM-5 (MFI structure) zeolite catalysts with Fe as the active center exhibit superior high-temperature activity and hydrothermal stability, making them one of the most promising systems. Research indicates that its catalytic performance strongly depends on the iron source precursor and preparation method. Both factors significantly influence catalytic activity and reaction mechanisms (E-R or L-H mechanisms) by regulating the morphology of active Fe species (isolated ions, oligomeric Fe_xO_y clusters, or oxide particles). Furthermore, introducing secondary metal components such as Ce, W, or Zr can generate synergistic effects. These effects optimize surface acidity, enhance redox capabilities, improve metal dispersion, and suppress excessive NH_3 oxidation, thereby further improving the catalyst's high-temperature catalytic performance and hydrothermal stability.

4. Beta Support

Compared to ZSM-5 with an MFI structure, Beta zeolite (BEA topology) demonstrates significant advantages in high-temperature NH_3-SCR catalysis due to its unique three-dimensional twelve-membered ring cross-linked pore system, higher specific surface area, and abundant acid site distribution [91–93]. Its larger pore dimensions provide a more favorable spatial environment for reactant diffusion and intermediate formation, making it particularly suitable for reactions involving macromolecules or requiring rapid mass transfer. Although its hydrothermal stability is generally considered slightly lower than that of mesoporous zeolites (e.g., CHA), Beta-based catalysts can maintain outstanding

catalytic activity and stability in the high-temperature range through rational metal modification and synthesis optimization [41]. This section systematically reviews research progress on single-metal and multi-metal catalysts supported on Beta zeolite, focusing on their catalytic performance, hydrothermal stability, and reaction mechanisms under high-temperature conditions.

4.1. Single Metal-Doped Beta Catalyst

Among various metal modification strategies for Beta zeolites, Fe has been the most extensively and deeply studied as an active center. Liu et al. [91] reported early on that Fe/Beta (SiO_2/Al_2O_3 = 25) catalysts prepared via the impregnation method could achieve NO conversion rates exceeding 95% within the 320~550 °C range (Figure 9). Subsequent work by Frey et al. [92] also demonstrated that Fe/Beta catalysts prepared via impregnation exhibit exceptionally high NH_3-SCR reactivity. Zhu et al. [93] employed the same preparation method to further investigate the influence of different Si/Al ratios (Si/Al = 9 and Si/Al = 19) on the NH_3-SCR performance of Fe/Beta catalysts. The study revealed that Fe/Beta catalysts with lower Si/Al ratios exhibit higher SCR activity. This is attributed to the increased acidity of zeolites with lower Si/Al ratios, which facilitates greater ammonia adsorption and activation on the catalyst surface. Furthermore, compared to Fe/Beta (Si/Al = 19), the Fe/Beta (Si/Al = 9) catalyst exhibited less aluminum leaching during hydrothermal aging, demonstrating superior hydrothermal stability.

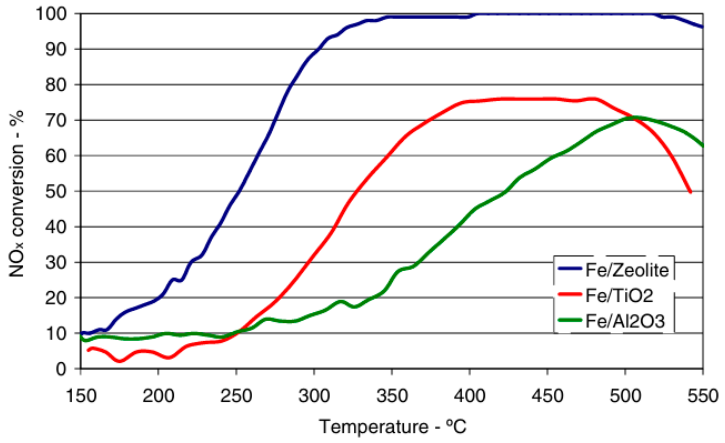

Figure 9. NH_3-SCR for Fe/Al_2O_3, Fe/TiO_2 and Fe/Beta zeolite. Reaction conditions: [NO] = [NH_3] = [CO] = 200 ppm, [C_3H_6] = 100 ppm, [SO_2] = 20 ppm, [O_2] = 12%, [H_2O] = [CO_2] = 4.5%, N_2 balance, GHSV = 45,000 h^{-1} [91].

In addition to the impregnation method, Fe/Beta catalysts can also be prepared via ion exchange. Ma et al. [94] compared the two methods and found that Fe/Beta catalysts prepared by ion exchange exhibited optimal activity, achieving nearly 100% NO_x conversion rates between 350~550 °C. The ion exchange method is more conducive than the impregnation method for generating more iron ions at ion exchange sites. Furthermore, the introduction of iron material does not significantly affect the surface area and pore volume of the ion exchange method samples, whereas the specific surface area and pore volume of Fe/Beta prepared by the impregnation method are relatively significantly reduced.

Liu et al. [95] also prepared Fe/Beta catalysts via ion exchange. They found that the catalytic activity of Fe/Beta increased with rising Fe loading, with the catalyst at 0.52 wt% Fe loading exhibiting outstanding performance, achieving NO conversion rates exceeding 90% across the 310~600 °C range. Kinetics experiments revealed that isolated Fe^{3+} species serve as the active sites for the NH_3-SCR reaction, while oligomers act as the active sites for NH_3 oxidation on the Fe/Beta catalyst. UV-vis results indicated that the Fe-0.52 sample

contained a higher concentration of isolated Fe^{3+}, thereby conferring the catalyst with enhanced catalytic activity. Additionally, NO_x conversion rates exhibit a slight decrease at elevated temperatures, particularly for the Fe-0.52 sample, where conversion rates drop by nearly 10% between 500 and 600 °C. This decline stems from excessive Fe loading, which increases oligomeric Fe_xO_y clusters. These clusters catalyze NH_3 oxidation, thereby impairing the catalyst's high-temperature activity.

Shi et al. [96] discovered that the presence of water vapor significantly enhances the NH_3-SCR performance of Fe-BEA catalysts. Under steam conditions, the Fe-BEA catalyst (Si/Al ≈ 20) exhibits NO_x conversion rates exceeding 80% across the 200~640 °C temperature range, demonstrating outstanding catalytic activity and N_2 selectivity surpassing 90% (Figure 10). Studies indicate that due to the abundance of Lewis acid sites on the Fe-BEA surface, the addition of water transforms these Lewis acid sites into Brønsted acid sites. This facilitates the adsorption of more NO_3^-/NO_2^- and NH_4^+ species onto the surface, thereby enhancing the catalyst's SCR activity. Furthermore, in situ DRIFTS studies confirm that both the L-H and E-R pathways coexist when water is present in the reaction feed stream.

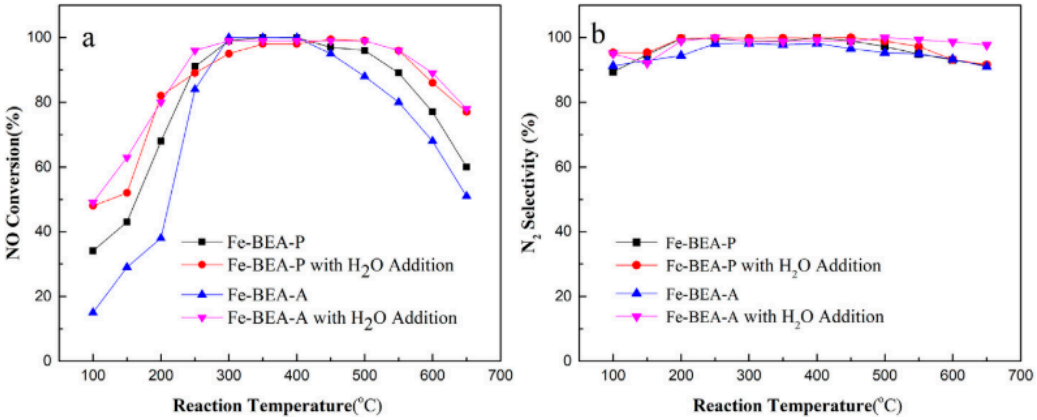

Figure 10. NO_x conversion (**a**) and N_2 selectivity (**b**) of Fe-BEA-P and Fe-BEA-A for the NH_3-SCR in the 100~650 °C range, Fresh and aged powder samples were denoted as Fe-BEA-P and Fe-BEA-A, respectively. Reaction conditions: [NO] = 350 ppm, [NH_3] = 385 ppm, [O_2] = 15%, [H_2O] = 8.5%, N_2 balance, GHSV = 60,000 h^{-1} [96].

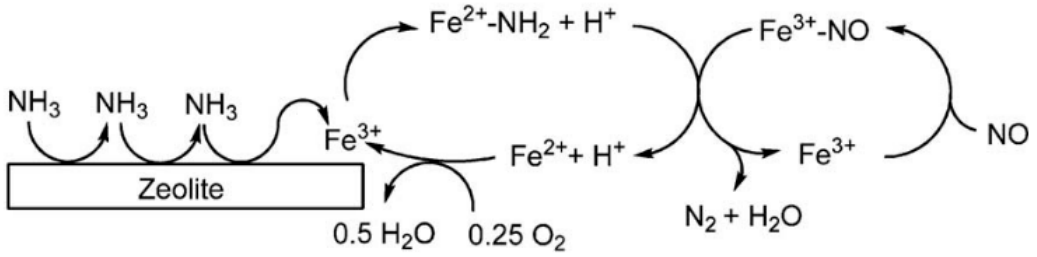

Figure 11. Mechanism of NH_3-SCR reaction on Fe/Beta zeolite catalyst [94].

The research group led by Klukowski [97] deduced the detailed SCR reaction mechanism of Fe/Beta catalysts (Figure 11). DRIFTS and NO_x-TPD analyses revealed that NO molecules adsorb on the catalyst surface to form Fe^{3+}-NO species, which then react with adsorbed NH_3. DRIFTS and NH_3-TPD confirmed that NH_3 primarily adsorbs on the Beta zeolite support. XANES results indicated that NH_3 can also adsorb on Fe^{3+} sites. On the Fe/Beta catalyst, NO and NH_3 adsorb simultaneously on adjacent Fe^{3+} sites. NH_3 undergoes multiple adsorption–desorption cycles on the zeolite support before ultimately adsorbing onto Fe^{3+} sites. The binding of NH_3 to Fe^{3+} sites causes partial reduction of these

sites, followed by oxidation cycles via O_2. Nevertheless, the reaction pathway involving isolated Fe^{3+} sites cannot be entirely ruled out.

4.2. Composite Metal-Doped Beta Catalyst

To further enhance the high-temperature activity of Fe/Beta catalysts, some researchers have attempted to incorporate small amounts of rare earth elements into Fe/Beta catalysts. Zhang et al. [41] prepared Ce-Fe/Beta catalysts using H-Beta (Si/Al = 25), $FeCl_2$, and $Ce(NO_3)_3$ as raw materials via an isovolumetric impregnation method. The study revealed that at a Ce doping level of 0.81%, the activity window of the Ce-Fe/Beta catalyst expanded to 311~683 °C (Figure 12a). Ce doping promoted the adsorption and activation of NO_x species, enhanced the adsorption capacity for NH_3 and NO, and increased the formation of reaction intermediates, thereby improving the NO_x removal activity of the Fe/Beta catalyst. After 24 h of hydrothermal aging at 750 °C (Figure 12b), the Fe/Beta catalyst exhibited the most significant performance decline, with NO_x conversion decreasing by approximately 12%. The Ce-Fe/Beta catalyst showed only a 3% reduction in NO_x conversion, indicating that Ce incorporation enhances the catalyst's hydrothermal stability. In situ DRIFTS experiments revealed coexistence of the L-H and E-R pathways in the SCR reaction, with the mechanism depicted in Figure 13. First, NO coordinated with hydroxyl groups forms HNO_2 species, which react with NH_3 at Lewis acid sites to generate intermediate NH_4NO_2. These intermediates readily decompose into N_2 and H_2O. Second, NH_4^+ at Brønsted acidic sites reacts with HNO_2 species to form NH_4NO_2, which subsequently decomposes into N_2 and H_2O. Third, NH_3 adsorbed at Lewis acid sites reacts with adsorbed oxygen to form surface amine species -NH_2 and -OH. The -NH_2 species reacts with gaseous NO to form NH_2NO, an unstable species that readily decomposes into N_2 and H_2O. Finally, NH_3 at Lewis acid sites reacts with NO_3^- species and -OH to form NH_4NO_3, which subsequently decomposes into N_2 and H_2O. The unstable NH_4NO_3 reacts with adsorbed NO to form NH_4NO_2 and NO_2, where NO_2 can further participate in reactions with NH_3 species, thereby achieving rapid SCR.

Sultana et al. [98] investigated the effects of different rare earth (La, Pr, Gd) modifications on Fe/Beta catalysts. The study found that the Gd-modified Gd-Fe/Beta catalyst exhibited optimal SCR activity, achieving NO_x conversion rates exceeding 95% within the 450~600 °C range (Figure 14). Moreover, the catalyst retained high hydrothermal stability even after hydrothermal aging at 800 °C. The incorporation of rare earth ions reduced the agglomeration of active iron species and stabilized the zeolite structure, thereby enhancing both SCR activity and hydrothermal stability. However, different methods for introducing rare earth cations into the zeolite matrix exerted varying effects on NO_x reduction activity. Therefore, Asima Sultana et al. incorporated Gd into Fe/Beta via co-ion exchange (CIE), subsequent ion exchange (SIE), impregnation (IMP), and physical mixing (PM) methods. The effects of different preparation methods on the activity of Gd-Fe/Beta catalysts were investigated. Figure 15 shows the SCR activity of these catalysts at 600 °C. The impregnation-prepared catalyst exhibited the highest activity, while the ion-exchange-prepared catalyst showed relatively lower activity. This activity difference likely stems from varying exchange amounts of Gd and Fe within the zeolite. In ion exchange, precise control of rare earth metal loading is challenging due to steric hindrance limitations in the liquid phase, where extensive hydrated metal cations form.

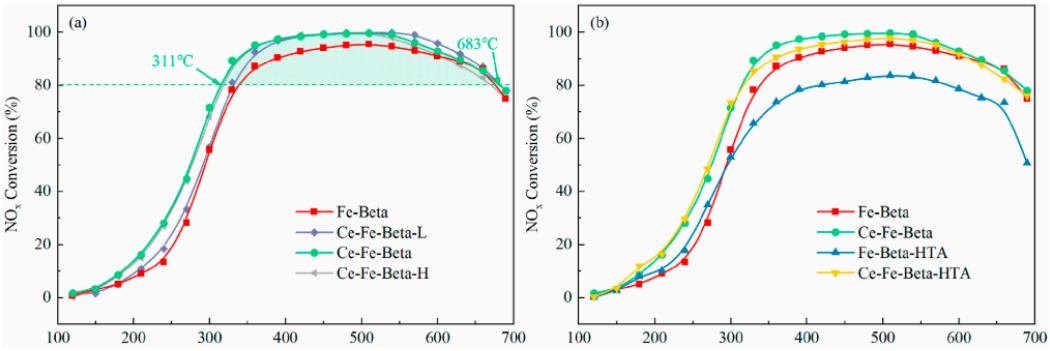

Figure 12. (**a**) Catalytic activity of different Ce doping amount; (**b**) Catalytic activity of before and after hydrothermal aging. Reaction conditions: [NO] = [NH_3] = 1000 ppm, [O_2] = [CO_2] = [H_2O] = 10%, N_2 balance, GHSV = 20,000 h^{-1} [41].

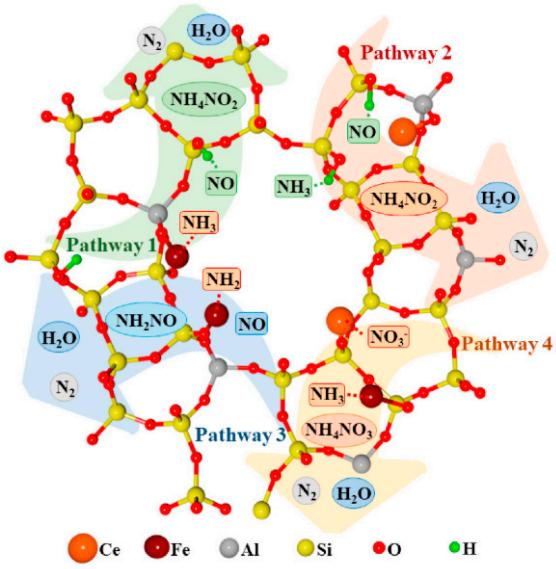

Figure 13. Proposed NH_3-SCR reaction pathway over Ce-Fe/Beta catalyst [41].

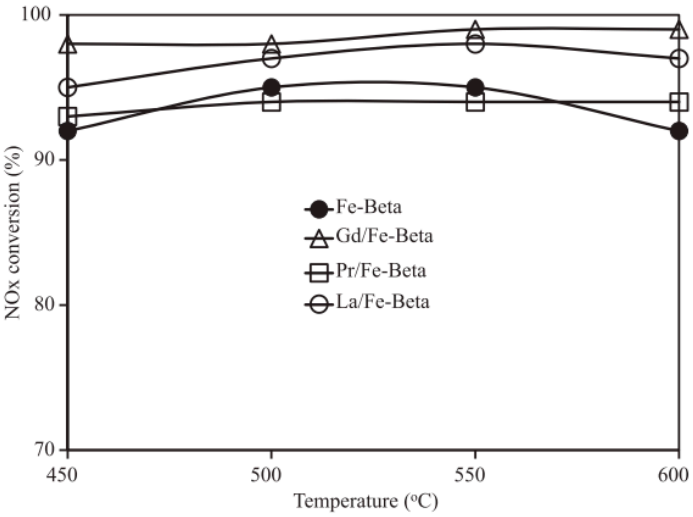

Figure 14. NO reduction activity of fresh Fe/Beta and rare earth modified Fe/Beta zeolite catalysts. Reaction conditions: [NO] = [NH_3] = 500 ppm, [O_2] = 16%, [H_2O] = 5.9%, He balance, GHSV = 125,000 h^{-1} [98].

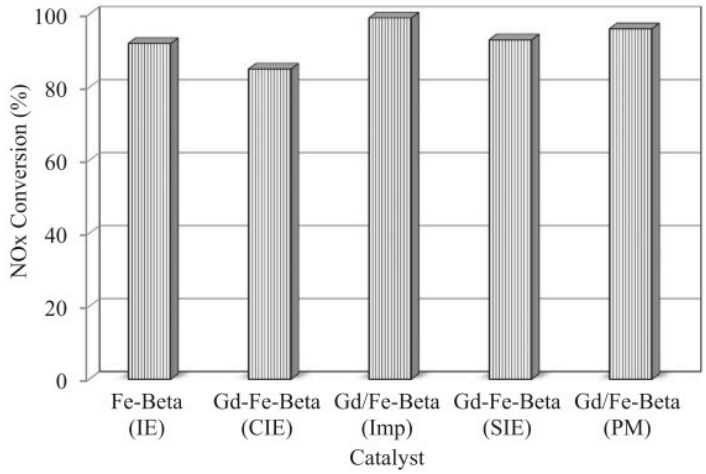

Figure 15. Effect of preparation method of Gd-Fe/Beta catalyst on NO reduction activity. Reaction conditions: [NO] = [NH_3] = 500 ppm, [O_2] = 16%, [H_2O] = 5.9%, He balance, GHSV = 125,000 h^{-1} [98].

In summary, Fe/Beta catalysts exhibit superior NH_3-SCR reactivity and stability compared to Fe/ZSM-5. Employing ion exchange techniques with Beta zeolites featuring relatively low Si/Al ratios as supports, and utilizing Fe as the primary active component supplemented with rare earth elements such as Ce and Gd, enhances the catalyst's high-temperature catalytic activity and hydrothermal stability. However, the highly complex structure of Beta zeolites (e.g., high defect density and presence of two polymorphic structures) adversely affects hydrothermal stability. Furthermore, the active sites and reaction mechanisms for NH_3-SCR on Fe/Beta catalysts require further confirmation, making it an unsuitable choice for fundamental research.

5. SSZ-13 Support

SSZ-13 (with CHA topology) is a mesoporous zeolite composed of silicon, aluminum, and oxygen, garnering significant attention due to its unique octahedral cage structure. Compared to macroporous zeolites such as MFI and BEA, zeolites with CHA structures not only possess high specific surface areas and abundant acid sites, but their uniform small pore diameters also confer exceptional molecular shape-selective catalytic capabilities. More importantly, the CHA framework exhibits exceptional stability under high-temperature hydrothermal conditions, effectively suppressing de-alumination and structural collapse. This property demonstrates significant application potential for high-temperature NH_3-SCR applications. This section systematically reviews recent research advances on single-metal and multi-metal modified SSZ-13 catalysts, focusing on the interaction between active metal species and the CHA framework, as well as the underlying catalytic reaction mechanisms.

5.1. Single Metal-Doped SSZ-13 Catalyst

Among single-metal-doped SSZ-13 catalysts, Fe and Cu represent the two most extensively studied and representative active sites, each exhibiting distinct advantages and challenges across different temperature ranges and reaction environments.

Fe/SSZ-13 catalysts have garnered significant attention for their outstanding high-temperature activity. However, the effective construction of their active sites remains a major challenge. Since the ionic diameter of hydrated Fe^{3+} (9 Å) [99] is significantly larger than the pore opening size of the CHA structure (3.8 Å) [59], conventional ion exchange struggles to introduce it into the channels. Therefore, iron precursors are typically maintained in the Fe^{2+} state during exchange under an inert atmosphere (e.g., N_2) to enhance exchange efficiency [100]. Gao et al. [101] successfully synthesized Fe/SSZ-13 catalysts using this strategy. At an Fe loading of 1.2 wt%, the catalyst achieved over 80% NO conver-

sion within the 350~550 °C temperature range. The study further indicates that different types of active iron species dominate at distinct temperature ranges: isolated Fe^{3+} ions serve as the active sites for low-temperature SCR reactions, while oligomeric iron clusters significantly contribute to high-temperature catalytic activity. Liu et al. [102] investigated the effects of calcination temperature on iron species distribution and catalytic performance in Fe/SSZ-13 catalysts through systematic characterization and kinetic analysis. Results indicate that while elevated calcination temperatures weaken low-temperature activity, they enhance high-temperature catalytic performance. This occurs because higher calcination temperatures induce slight aggregation of isolated Fe^{3+} ions into dimers or oligomeric iron clusters, thereby boosting high-temperature activity (achieving over 90% NO conversion within the 380~575 °C range). Additionally, Chen et al. [103] discovered that treating SSZ-13 zeolite with HNO_3 releases Brønsted acid sites partially covered by Fe_xO_y species and removes some framework aluminum to form strong Lewis acid sites, further optimizing catalytic performance. Although the aforementioned methods enhance the activity of Fe/SSZ-13 catalysts, their preparation processes remain relatively complex, and their high-temperature hydrothermal stability still requires improvement. These factors limit their large-scale industrial application to some extent.

In addition to Fe-based SSZ-13 catalysts, Cu-based systems have also become a research focus due to their broader active temperature window and superior catalytic performance. Early studies by Kwak et al. [104] demonstrated that Cu/SSZ-13 exhibits significantly higher activity than Cu/ZSM-5 and Cu/Beta molecular sieves, maintaining over 80% NO_x conversion efficiency between 200~550 °C. Its performance is highly dependent on the morphology and distribution of Cu species. Research indicates that preparation methods decisively influence the state of Cu species. For instance, Han et al. [105] discovered that catalysts synthesized via hydrothermal methods exhibit more stable Cu^{2+} sites within the hexagonal ring structure compared to those prepared by impregnation or ion exchange. These catalysts also demonstrate stronger adsorption capacities for NH_3 and NO, resulting in superior and stable catalytic activity across the 215~600 °C temperature range. Furthermore, the choice of copper precursor directly governs Cu^{2+} placement and catalytic behavior. Wang et al. [106] systematically compared the effects of different copper sources ($Cu(NO_3)_2$, $CuSO_4$, $CuCl_2$, and $Cu(CH_3COO)_2$). They found that when using $Cu(NO_3)_2$ and $CuSO_4$, Cu^{2+} predominantly distributed in octahedral sites; while Cu^{2+} preferentially localized in the hexagonal ring with $CuCl_2$ and $Cu(CH_3COO)_2$, the latter facilitating Cu^{2+}/Cu^{+} redox cycling due to stronger charge displacement. All catalysts achieved over 90% NO conversion and near-100% N_2 selectivity across the 200~680 °C temperature range (Figure 16). Notably, hydrothermal treatment induces Cu species restructuring, promoting CuO formation and enhancing NO_x adsorption. This paradoxically boosts high-temperature activity while shifting the reaction pathway from the L-H mechanism to the E-R mechanism (Figure 17).

In summary, by optimizing preparation strategies and precursor selection, the chemical environment and spatial distribution of Cu species within SSZ-13 can be precisely controlled, yielding Cu/SSZ-13 catalysts that combine a broad active window with high hydrothermal stability. However, further in situ characterization is required to elucidate the reaction mechanism and species dynamics evolution.

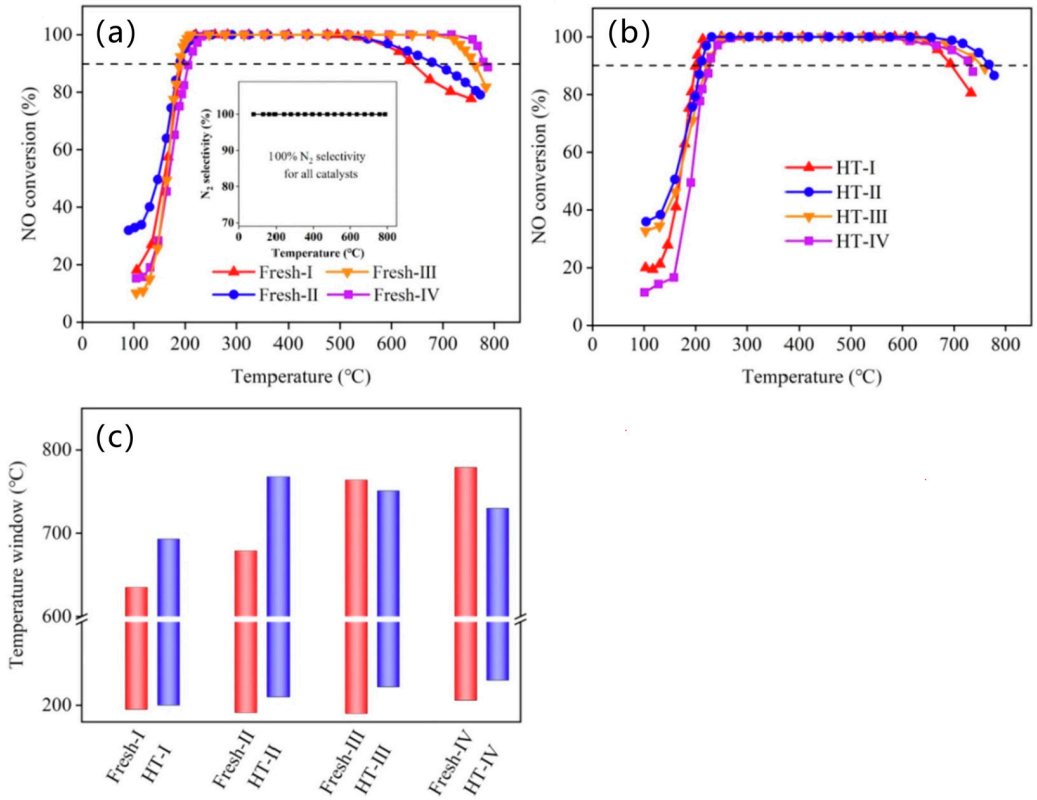

Figure 16. The NO conversion and N_2 selectivity of the (**a**) fresh catalysts, (**b**) aged catalysts, and (**c**) the temperature window of over 90% of NO conversion for the fresh and aged catalysts. Reaction condition: [NO] = [NH_3] = 1000 ppm, [O_2] = 5%, N_2 balance, GHSV = 130,000 h^{-1} [106].

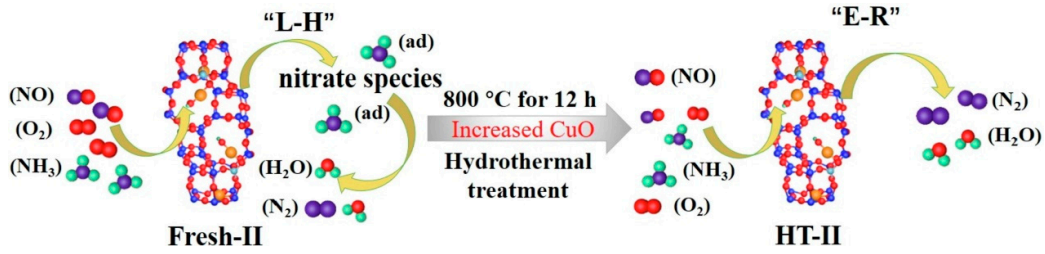

Figure 17. The SCR reaction mechanism of the Fresh-II and HT-II catalysts [106].

5.2. Composite Metal-Doped SSZ-13 Catalyst

The high-temperature activity and hydrothermal stability of single metal modified SSZ-13 catalysts remain limited. Consequently, introducing a second metal to form bifunctional active sites has emerged as an effective modification strategy [107–109]. Depending on the core function of the second metal, its primary roles can be categorized into two types: first, stabilizing the zeolite framework and suppressing sintering of the active components [110–113]; second, introducing new active sites and synergistically broadening the catalytic temperature window [114–118]. It is worth noting that multiple metal modifiers can simultaneously possess both functions, thereby synergistically enhancing the overall performance of the catalyst.

Among these, Zr serves as a typical representative for stabilizing the framework and suppressing sintering. Research by Chen et al. [110] indicates that introducing Zr significantly enhances the hydrothermal stability of Fe/SSZ-13 catalysts. After harsh hydrothermal aging at 750 °C, the activity of unmodified Fe/SSZ-13 declined sharply, whereas Zr-Fe/SSZ-13 (especially at a Zr loading of 0.31 wt%) maintained over 90% NO conversion efficiency within the 430~575 °C range. Characterization analyses indicate that Zr introduc-

tion optimizes Fe species dispersion, effectively suppressing migration and sintering during hydrothermal aging, thereby stabilizing the catalyst structure. Furthermore, in situ DRIFTS studies reveal that the SCR reaction on Fe/SSZ-13 and Zr-Fe/SSZ-13 catalysts proceeds via three pathways (Figure 18). Zr doping did not alter the SCR reaction pathways. It not only promoted Fe dispersion and the formation of more active sites but also enhanced NH_3 and NO adsorption and the formation of reaction intermediates (such as -NH_2, -HNO_2, and -NO_2), thereby positively promoting the reaction.

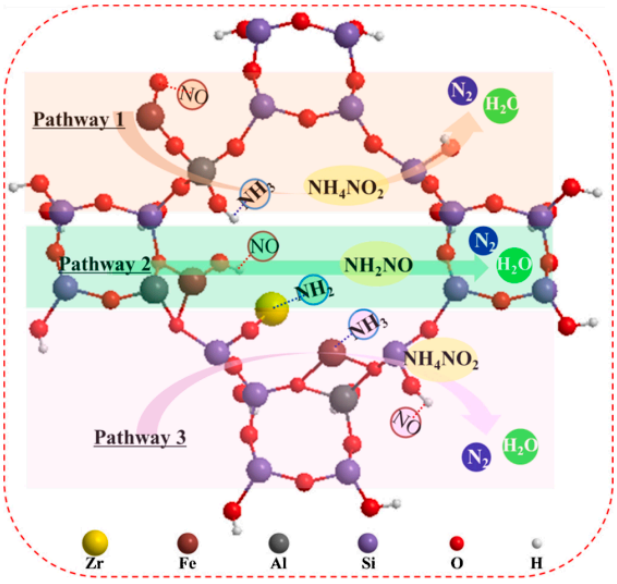

Figure 18. Proposed NH_3-SCR reaction pathway over Zr-Fe/SSZ-13 catalyst [110].

In addition to the aforementioned Zr, Ti and Zn are also typical elements dedicated to stabilizing the structure. Liu et al. [111] found that post-treatment modification of Cu/SSZ-13 with $TiCl_4$ solution resulted in an optimized Ti-Cu/SSZ-13 catalyst capable of achieving over 90% NO_x conversion efficiency between 250~640 °C, while exhibiting excellent hydrothermal stability. The incorporation of Ti increases TiO_2 content within the zeolite, where highly dispersed TiO_2 facilitates high-temperature denitrification reactions. Moreover, Ti partially protects the zeolite framework during high-temperature hydrothermal processes, conferring exceptional hydrothermal stability. Particularly noteworthy is the behavior of zinc. Although Zn is considered toxic in certain scenarios, Xu et al. [112] discovered that incorporating Zn into the Cu/SSZ-13 system via a one-pot method yields a high-performance catalyst. It achieves over 90% NO_x conversion between 200~600 °C and exhibits significantly superior hydrothermal stability compared to conventional Cu/SSZ-13 (Figure 19). Mechanism studies (Figure 20) indicate that Zn formation creates more stable complexes such as [Zn-OH]-Z and [Cu-O-Zn]-Z. These complexes act as "anchor points," effectively suppressing Cu^{2+} ion migration and sintering during high-temperature hydrothermal aging, thereby stabilizing the catalytic structure.

In addition to transition metal doping, rare earth element doping exhibits similar effects. Addressing the insufficient hydrothermal stability of high-aluminum Cu/SSZ-13 catalysts, Zhao et al. [113] proposed modifying the Cu/SSZ-13 catalyst by introducing different rare earth ions (Ce, La, Sm, Y, Yb). Results indicate that among all tested rare earth elements, Y exhibits the most pronounced effect. Y effectively stabilizes the alumina framework of the molecular sieve, protects Brønsted acid sites, and promotes the preferential occupation of Cu^{2+} ions at highly stable hexagonal ring sites. This significantly enhances the catalyst's NH_3-SCR activity and stability after harsh hydrothermal aging at 800 °C.

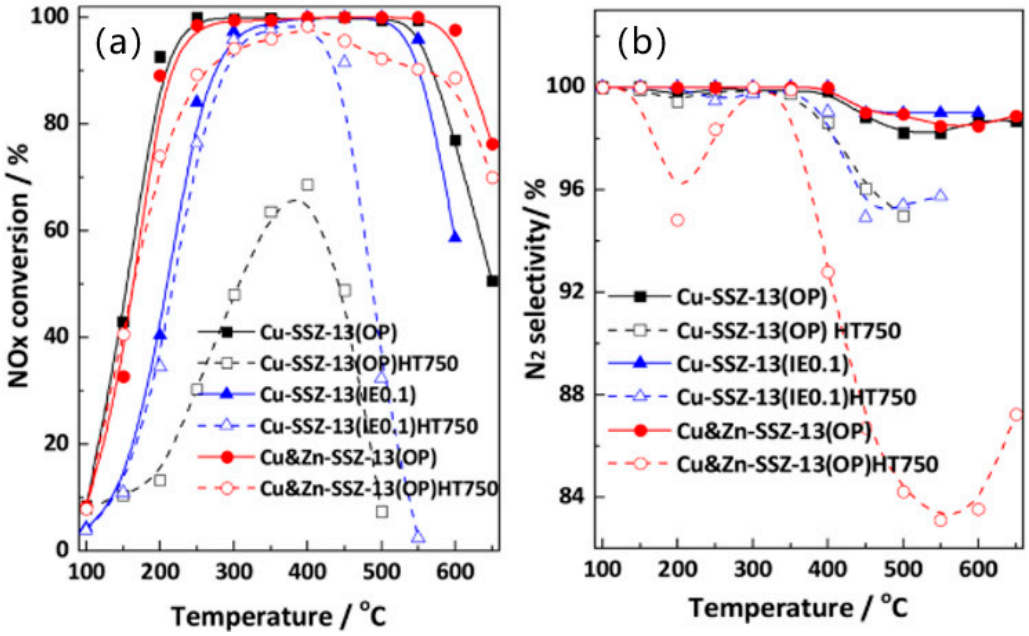

Figure 19. (**a**) Light-off NH_3-SCR curves over the zeolite catalysts; (**b**) N_2 selectivity. Reaction conditions: [NO] = [NH_3] = 600 ppm, [O_2] = 6%, [H_2O] = 5%, He balance, GHSV ≈ 400,000 h^{-1} [112].

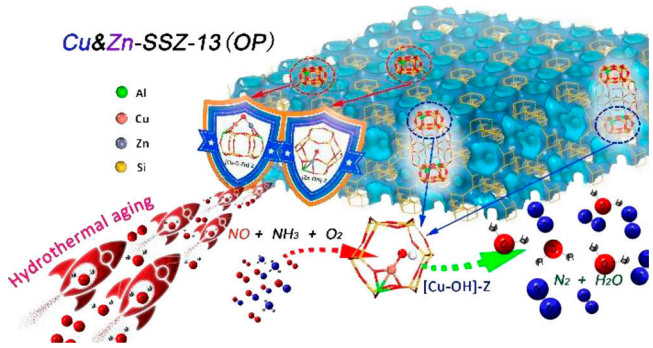

Figure 20. Schematic diagram of hydrothermal aging resistance of Cu-Zn/SSZ-13 [112].

Unlike the metals used for structural stabilization mentioned above, another class of research focuses on synergistic effects achieved by introducing metals with variable valence states. This approach creates new high-temperature active sites, thereby further expanding the temperature window. In this regard, Fe and Nb demonstrate significant potential. Fe species not only offer low cost but also introduce highly effective high-temperature active sites into the system. Studies [114–116] demonstrate that incorporating Fe—whether via the one-pot method or ion exchange—significantly enhances the catalyst's high-temperature performance, enabling it to maintain over 90% NO conversion across a broad temperature range of 200~625 °C (Figure 21). Research further indicates that H_2O presence may enhance high-temperature activity by suppressing non-selective NH_3 oxidation. This performance boost stems from synergistic and complementary active sites: isolated Cu^{2+} species dominate low-temperature SCR reactions, while introduced monomeric Fe^{3+} species serve as highly efficient high-temperature active centers. This synergistic effect significantly broadens the operational temperature window of Fe-Cu/SSZ-13 compared to single Cu systems. However, it is important to note that Fe loading has an optimal value; excessive doping leads to destruction of the zeolite structure and formation of inactive Fe_2O_3 clusters, resulting in performance degradation.

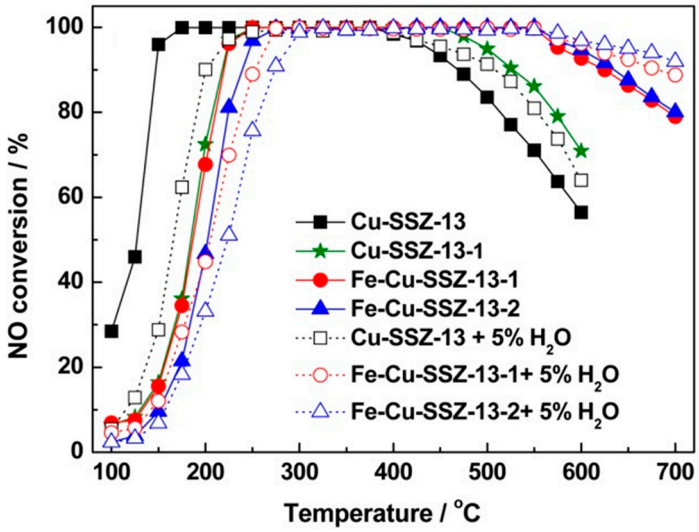

Figure 21. NO conversion as a function of temperature over Cu/SSZ-13 and Fe-Cu/SSZ-13 catalysts. Reaction conditions: [NO] = [NH_3] = 1000 ppm, [O_2] = 3%, [H_2O] = 5%, N_2 balance, GHSV = 50,000 h^{-1} [114].

Nb exhibits multiple valence states and demonstrates significant potential similar to Fe in providing new active sites and synergistic effects. Studies by Wang et al. [117] and Liu et al. [118] both confirm that introducing Nb significantly broadens the activity window of Cu/SSZ-13. For instance, after loading 0.7 wt% Nb, the temperature window for the $Nb_{0.7}$-Cu_2/SSZ-13 catalyst achieving >90% NO_x conversion expanded from 275~580 °C to 200~625 °C; while Nb modification of the catalyst with the optimal Cu loading (2.8 wt%) substantially enhanced its high-temperature performance (Figure 22b), extending the active window to 700 °C. This enhancement primarily stems from two mechanisms: First, the formation of Nb=O significantly increases the number of Lewis and Brønsted acid sites on the catalyst surface, enhancing NH_3 adsorption capacity; Second, Nb introduction optimized Cu species distribution, increasing the number of active Cu^{2+} sites and thereby enhancing overall redox capability. In situ DRIFTS studies confirmed that both Cu/SSZ-13 and Nb-Cu/SSZ-13 catalysts follow the L-H mechanism (Figure 23).

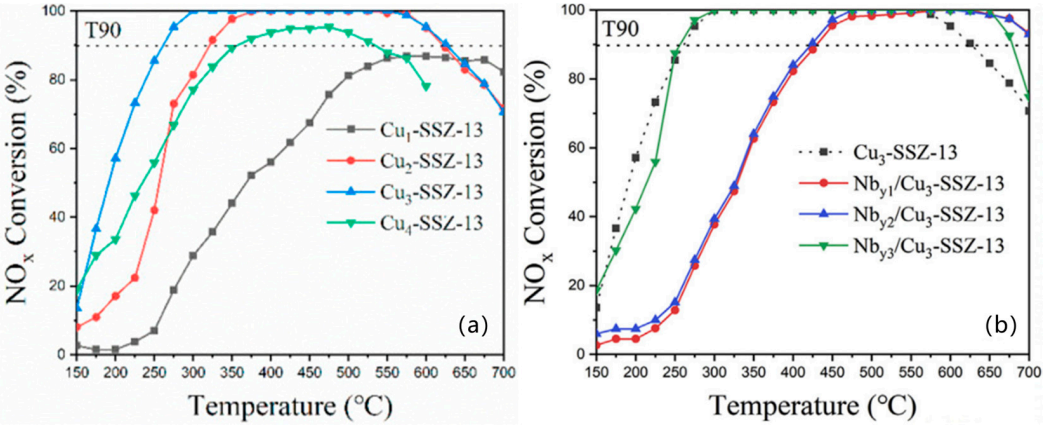

Figure 22. (**a**) The NO_x conversion on Cu/SSZ-13 catalysts with various Cu loadings; (**b**) The NO_x conversion of Cu_3/SSZ-13 and Nb_y-Cu_3/SSZ-13 (y = 1,2,3). Reaction conditions: [NO] = [NH_3] = 500 ppm, [O_2] = 5%, [H_2O] = 5%, N_2 balance, GHSV = 60,000 h^{-1} [118].

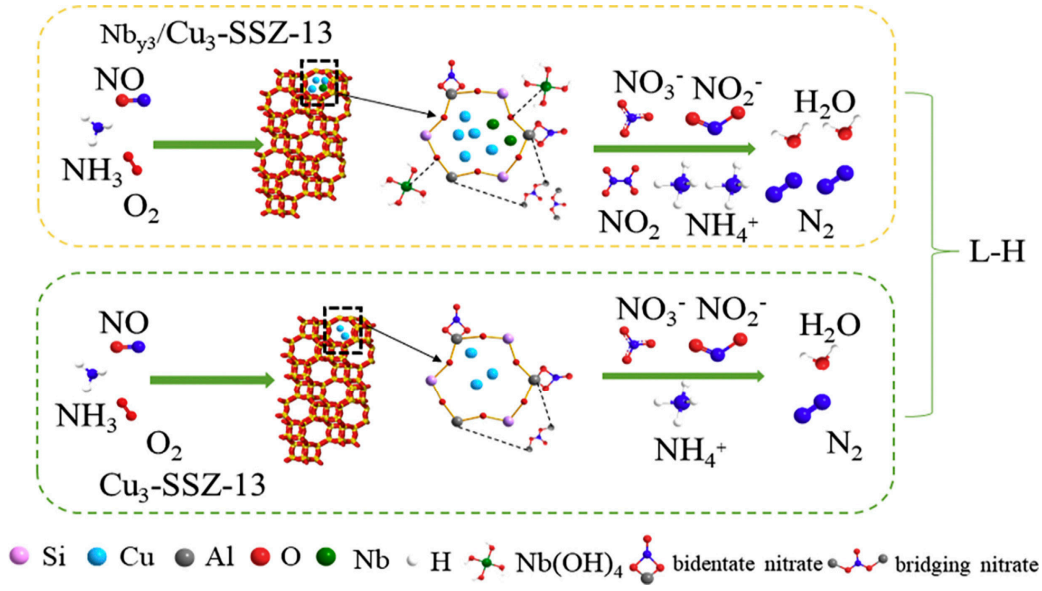

Figure 23. The catalytic mechanism of the Cu_3/SSZ-13 and Nb_{y3}-Cu_3/SSZ-13 in NH_3-SCR reaction [118].

In summary, modifying SSZ-13 with secondary metals—whether for structural stabilization (e.g., Zr, Ti, Zn, Sm) or synergistic enhancement (e.g., Fe, Nb)—significantly improves its high-temperature catalytic performance and hydrothermal stability. These strategies offer diverse and viable pathways for designing efficient SCR catalysts tailored to the extreme operating conditions of gas turbines.

6. SAPO-34 Support

As discussed in Section 5, SAPO-34 with its CHA topology also exhibits core advantages such as high hydrothermal stability and shape-selective catalysis [119–122]. However, its unique silicon-phosphorus-aluminum (SAPO) framework endows it with physicochemical properties distinct from SSZ-13, most notably milder framework acidity. This section focuses on research progress concerning SAPO-34-based catalysts, emphasizing the structure and reaction mechanisms of single-metal active sites represented by Cu and Fe. It also analyzes the synergistic optimization mechanisms of composite metal doping on their activity distribution, redox performance, and hydrothermal stability.

6.1. Single Metal-Doped SAPO-34 Catalyst

Currently, research on single-metal-doped SAPO-34 catalysts has primarily focused on Cu-based systems, with most employing ion exchange methods for preparation. Although Fe-based zeolites typically exhibit excellent catalytic activity and hydrothermal stability at high temperatures, SAPO-34, being a mesoporous zeolite similar to SSZ-13, presents significant steric hindrance to Fe^{3+} ion incorporation due to its pore structure. This hindrance makes it difficult to effectively load iron active sites using conventional ion exchange methods. To address this, some researchers have developed a one-pot hydrothermal synthesis strategy to directly incorporate Fe species into the SAPO-34 framework. This method not only offers a simple process with good reproducibility but also allows flexible control over the loading amount of active components, making it more conducive to constructing efficient SCR catalysts with a wide temperature window. For instance, the one-pot Fe/SAPO-34 catalyst (Fe loading: 1.03 wt%) synthesized by Andonova et al. [123] achieved over 80% NO_x conversion within the 300~600 °C range. Notably, during hydrothermal aging, migration of Fe species formed more stable active sites, further enhancing catalytic activity.

However, due to the relatively complex synthesis process of Fe/SAPO-34, related research remains far less extensive than that on Cu-based systems. Although Cu/SAPO-34 catalysts exhibit high activity and N_2 selectivity in the low-to-medium temperature range (e.g., around 200 °C), their high-temperature performance often declines significantly due to excessive NH_3 oxidation. As reported by Wang et al. [124], Cu/SAPO-34 achieves a NO conversion rate of 95% at 200 °C, but its activity continuously declines with increasing temperature, reaching only about 60% at 600 °C.

To improve the high-temperature performance of Cu/SAPO-34, researchers have explored various preparation methods. Zhang et al. [125] successfully synthesized a Cu/SAPO-34 catalyst with over 90% activity across 260~575 °C using solid-state ion exchange. Tang et al. [126] achieved NO conversion rates exceeding 80% between 200~600 °C for Cu/SAPO-34 obtained via a one-pot method. Wang et al. [127] employed a one-step hydrothermal synthesis to prepare Cu/SAPO-34 on cordierite support. At a space velocity of 12,000 h^{-1}, it exhibited nearly 100% NO conversion between 300~670 °C, demonstrating outstanding high-temperature activity and hydrothermal stability. This indicates that optimizing preparation methods can effectively broaden the operating temperature window and enhance high-temperature sintering resistance. Zhang et al. [125] investigated the reaction mechanism on Cu/SAPO-34 catalysts, revealing that the L-H mechanism dominates on these catalysts (Figure 24).

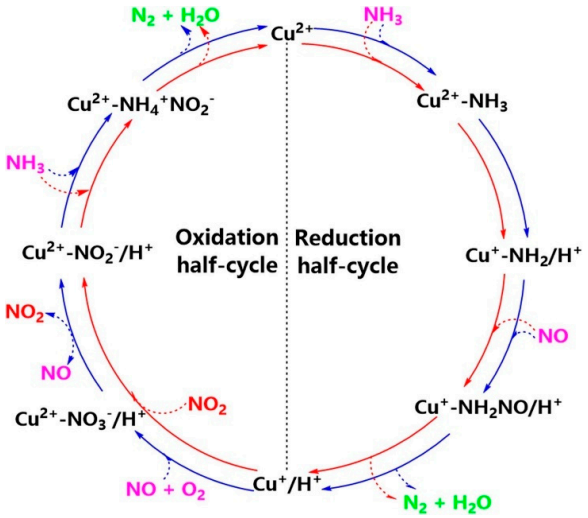

Figure 24. NH_3-SCR reaction mechanisms over Cu/SAPO-34 [125].

6.2. Composite Metal-Doped SAPO-34 Catalyst

To enhance the high-temperature NH_3-SCR performance of Cu/SAPO-34 catalysts, introducing a second metal to construct bifunctional active sites has become a key strategy. Studies indicate that doping with metals such as Fe and Ce can significantly modulate the distribution of catalytic active sites, surface acidity, and redox capabilities, thereby synergistically enhancing both broad-temperature catalytic activity and hydrothermal stability.

Zhao et al. [128] incorporated Fe into Cu/SAPO-34 via impregnation. They found that appropriate Fe loading promotes the transformation of bulk CuO into isolated Cu^{2+} sites while introducing additional isolated Fe^{3+} active sites. This enables Fe-Cu/SAPO-34 to maintain NO_x conversion rates above 80% across the 200~550 °C range. The Cu-Fe/SAPO-34 catalyst prepared by ion exchange by Doan et al. [129] exhibited NO_x conversion rates exceeding 90% across the broad temperature range of 250~600 °C, maintaining a 95% removal rate even at 600 °C (Figure 25). The coexistence of Fe and Cu not only enhances the surface acidity of the catalyst and promotes NH_3 adsorption but also provides more

isolated Cu^{2+} and oligomeric Fe_xO_y species, thereby broadening the active temperature window.

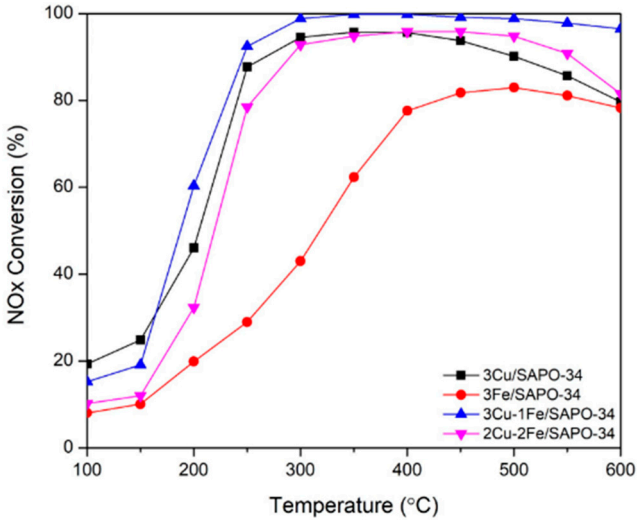

Figure 25. NO_x conversion during standard NH_3-SCR as a function temperature of the Cu-Fe/SAPO-34 and comparison of all catalyst samples. Reaction conditions: [NO] = [NH_3] = 1000 ppm, [O_2] = 8%, GHSV = 120,000 h^{-1} [129].

On the other hand, the introduction of the rare earth element Ce has also been proven to be an effective approach for enhancing high-temperature performance. Wang et al. [130] found that Ce modification significantly enhances the NO removal capacity of Cu/SAPO-34 in the high-temperature range of 375~570 °C. Mechanistic studies indicate that Ce doping increases the surface acidity, Cu^+/Cu^{2+} ratio, and NO adsorption-oxidation capability of the catalyst. Mao et al. [131] further investigated Ce's impact on hydrothermal stability, noting that Ce introduction helps stabilize the CHA framework, maintain medium-to-weak acidic sites, and suppress Cu species migration and agglomeration. Optimal Ce loading (e.g., Cu/Ce mass ratio of 4:5) effectively mitigates activity decline and structural damage caused by hydrothermal aging at 750 °C.

However, current research on SAPO-34 catalysts remains predominantly focused on the low-to-medium temperature range, with limited studies reported for the high-temperature range. Moreover, the reaction mechanism of SAPO-34 catalysts under high-temperature conditions remains unclear. Consequently, SAPO-34 supports are not an optimal choice for high-temperature denitrification applications.

7. Other Support

The preceding sections have systematically explored the application of mainstream zeolite supports such as ZSM-5, Beta, SSZ-13, and SAPO-34 in high-temperature NH_3-SCR systems. To broaden the catalytic material portfolio, researchers continue to develop zeolites featuring novel topologies, unique acidities, or improved economic viability to overcome existing performance limitations. This chapter summarizes several emerging or niche zeolite materials with development potential beyond the aforementioned mainstream supports (as shown in Table 2). Although related research remains in its developmental stage, these materials have demonstrated unique advantages in aspects such as activity windows, hydrothermal stability, or synthesis costs, offering new avenues for designing high-temperature SCR catalysts.

Table 2. Preparation conditions and SCR performance of other emerging zeolite supported catalysts.

Catalyst	Preparation Method	Reaction Condition	Denitrification Activity	Refs.
Cu/SSZ-16	ion-exchange	[NO] = [NH_3] = 600 ppm, [O_2] = 6%, [H_2O] = 5%, GHSV = 400,000 h^{-1}	(300~670 °C) > 95%	[132]
Cu/SSZ-16	ion-exchange	[NO] = [NH_3] = 500 ppm, [O_2] = 5%, [H_2O] = 5%, GHSV = 100,000 h^{-1}	(175~600 °C) > 90%	[133]
Cu/UZM-9	ion-exchange	[NO] = [NH_3] = 500 ppm, [O_2] = 5%, [H_2O] = 10%, GHSV = 100,000 h^{-1}	(250~700 °C) > 90%	[134]
Cu/SSZ-39	ion-exchange	[NO] = [NH_3] = 500 ppm, [O_2] = 5%, [H_2O] = 5%, GHSV = 190,000 h^{-1}	(250~550 °C) > 90%	[135]
Cu/SSZ-39	ion-exchange	[NO] = [NH_3] = 500 ppm, [O_2] = 5%, [H_2O] = 5%, GHSV = 200,000 h^{-1}	(200~550 °C) > 90%	[136]
Cu/ZJM-7	ion-exchange	[NO] = [NH_3] = 500 ppm, [O_2] = 5%, [H_2O] = 5%, GHSV = 80,000 h^{-1}	(200~550 °C) > 90%	[137]
Cu/SUZ-4	ion-exchange	[NO] = [NH_3] = 500 ppm, [O_2] = 5%, [H_2O] = 5%, GHSV = 200,000 h^{-1}	(250~550 °C) > 90%	[138]
Cu/LTA	ion-exchange	[NO] = [NH_3] = 500 ppm, [O_2] = 5%, [H_2O] = 10%, GHSV = 100,000 h^{-1}	(220~600 °C) > 90%	[139]
Cu/ERI	ion-exchange	[NO] = [NH_3] = 500 ppm, [O_2] = 5%, [H_2O] = 3%, GHSV = 50,000 h^{-1}	(250~600 °C) > 90%	[140]
Fe/SSZ-39	one-pot	[NO] = 50 ppm, [NH_3] = 60 ppm, [O_2] = 10%, [H_2O] = 10%	(330~550 °C) > 90%	[141]
Fe/UZM-35	one-pot	[NO] = [NH_3] = 500 ppm, [O_2] = 5%, [H_2O] = 10%, GHSV = 100,000 h^{-1}	(250~600 °C) > 90%	[142]
Fe/MCM-56	ion-exchange	[NO] = [NH_3] = 2500 ppm, [O_2] = 2.5%	(430~600 °C) > 80%	[143]
Cu/SAPO-18	incipient wetness impregnation	[NO] = 1000 ppm, [NH_3] = 1100 ppm, [O_2] = 5%, [H_2O] = 10%, GHSV = 30,000 h^{-1}	(230~575 °C) > 80%	[144]
Ce-Cu/SAPO-18	ion-exchange	[NO] = [NH_3] = 500 ppm, [O_2] = 14%, [H_2O] = 5%, GHSV = 130,000 h^{-1}	(200~600 °C) > 90%	[145]
Cu/SAPO-44	ion-exchange	[NO] = [NH_3] = 500 ppm, [O_2] = 5.3%, [H_2O] = 10%, GHSV = 100,000 h^{-1}	(200~550 °C) > 90%	[146]
Cu/SAPO-47	ion-exchange	[NO] = [NH_3] = 500 ppm, [O_2] = 5%, [H_2O] = 5%, GHSV = 100,000 h^{-1}	(250~600 °C) > 90%	[147]
Cu/SAPO-18/34	incipient wetness impregnation	[NO] = 1000 ppm, [NH_3] = 1100 ppm, [O_2] = 5%, [H_2O] = 10%, GHSV = 30,000 h^{-1}	(200~575 °C) > 90%	[148]

As shown in Table 2, small-pore zeolites such as SSZ-16 (AFX) and UZM-9 (LTA) demonstrate outstanding potential in high-temperature SCR. Among these, the performance of the Cu/SSZ-16 catalyst is particularly noteworthy. Research by Chen et al. [132] systematically investigated the impact of Cu loading on SSZ-16 performance. The study revealed that at a Cu loading of 2.21 wt% ($Cu_{0.091}$/SSZ-16), the catalyst achieves > 95% NO conversion within the 300~670 °C temperature window. Notably, even samples with low Cu loading maintained 90% activity at the extreme high temperature of 700 °C (Figure 26a), with nearly all samples exhibiting N_2 selectivity close to 100% (Figure 26b). This outstanding high-temperature performance stems from its unique resistance to Cu species sintering (inhibiting the conversion of $[CuOH]^+$ to CuO_x) and relatively weak NH_3 adsorption strength, effectively suppressing non-selective NH_3 oxidation. However, the hydrothermal stability of the catalyst is critical for practical applications. After aging at 650 °C and 750 °C [133], the Cu/SSZ-16 catalyst exhibited minimal activity loss due to the retention of more active Cu^{2+}-2Z species; However, when the calcination temperature reached 850 °C, the AFX framework collapsed. The interaction between active Cu species and the framework weakened, leading to their conversion into inactive CuO_x and $Cu(AlO_2)_2$ species, resulting in a sharp decline in activity (Figure 27).

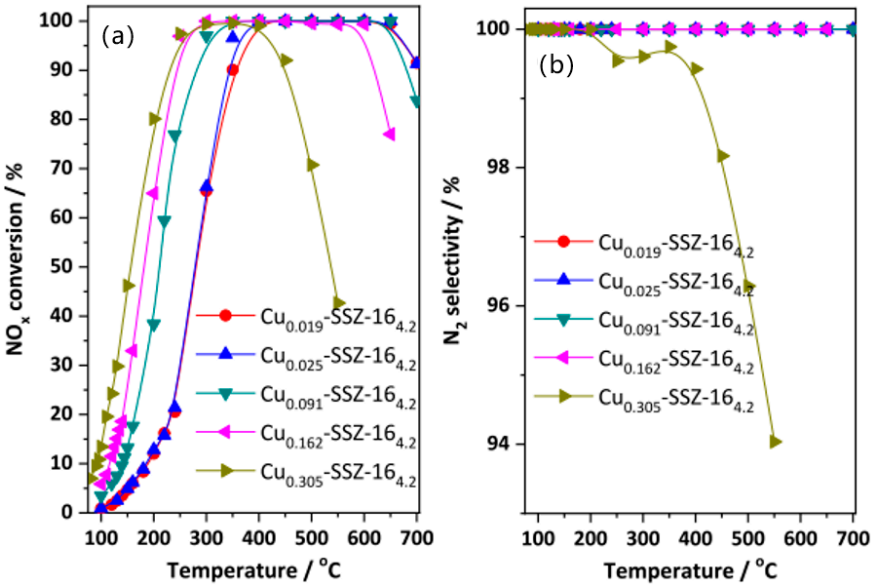

Figure 26. (**a**) Light-off curves for the NH_3-SCR; (**b**) N_2 selectivity over Cu/SSZ-16 catalysts with different Cu loadings. Reaction conditions: [NO] = [NH_3] = 600 ppm, [O_2] = 6%, [H_2O] = 5%, He balance, GHSV = 400,000 h^{-1} [132].

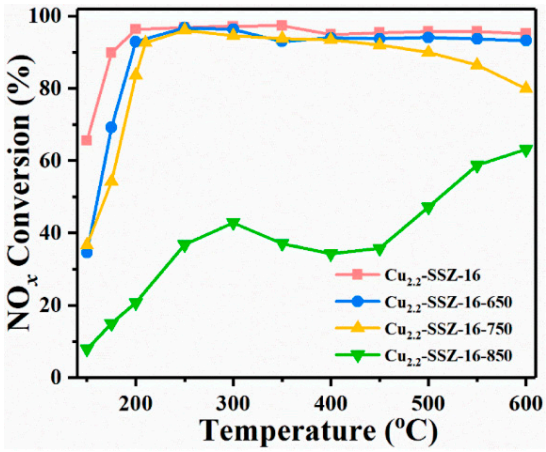

Figure 27. NO_x conversion as a function of temperature in NH_3-SCR reaction over $Cu_{2.2}$/SSZ-16 at different aging temperature of 650, 750 and 850 °C. Reaction conditions: [NO] = [NH_3] = 500 ppm, [O_2] = [H_2O] = 5%, N_2 balance, GHSV = 100,000 h^{-1} [133].

Compared to SSZ-16, UZM-9 also exhibits a broad activity window. The Cu/UZM-9 (2.90 wt%) catalyst prepared by Wei et al. [134] achieved NO conversion rates >90% within the 250~700 °C range, reaching 100% between 300 and 600 °C (Figure 28a). However, the formation of the byproduct N_2O increases significantly at high Cu loadings (Figure 28b), posing challenges to its N_2 selectivity.

Among the SAPO family members excluding SAPO-34, SAPO-18 with an AEI topology has drawn attention due to its similarity to the CHA structure [144]. However, single Cu modification exhibits limited high-temperature performance, prompting researchers to frequently employ rare earth element doping for optimization. Research by Han [145] and Gao [149] et al. indicates that among various rare earth elements, Ce exhibits the most pronounced modification effect. The Ce-Cu/SAPO-18 catalyst prepared by introducing 1.24 wt% Ce achieves over 90% NO conversion within the 200~600 °C range, with N_2 selectivity approaching 100% (Figure 29). Mechanistic studies reveal that Ce doping promotes the migration of active Cu^{2+} species to energetically favorable positions, thereby enhancing catalytic activity. Concurrently, Ce mitigates framework hydrolysis during

hydrothermal aging, significantly improving catalyst durability. In situ DRIFTS results indicate that reactions on this catalyst follow a mixed L-H and E-R mechanism, with the lower-energy L-H pathway dominating.

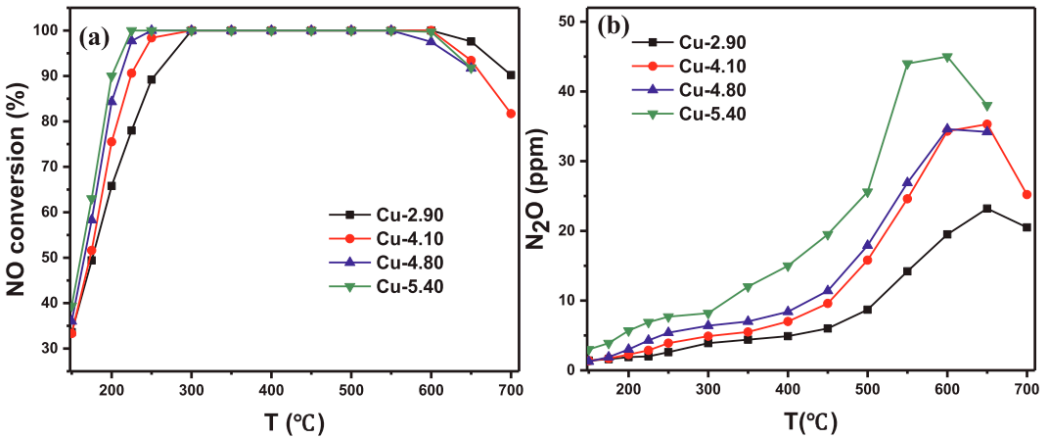

Figure 28. (**a**) The conversion of NO and (**b**) the concentration of N_2O in the product stream as a function of temperature in NH_3-SCR reaction over Cu-2.90, Cu-4.10, Cu-4.80, and Cu-5.40 catalysts. Reaction conditions: [NO] = [NH_3] = 500 ppm, [O_2] = 5%, [H_2O] = 10%, N_2 balance, GHSV = 100,000 h^{-1} [134].

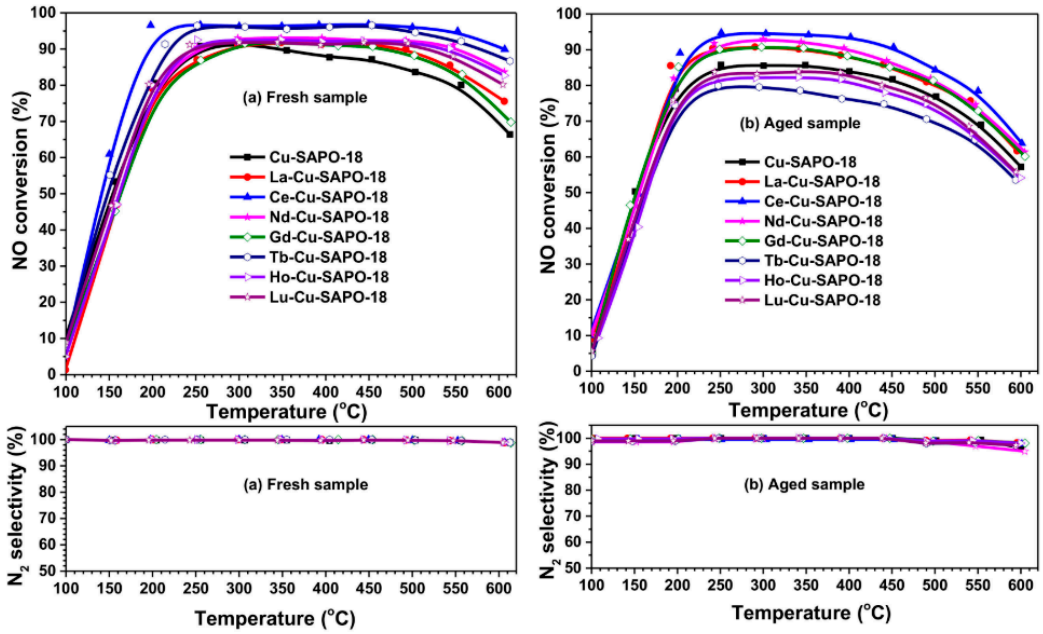

Figure 29. NO conversion and N_2 selectivity as a function of temperature for the selective catalytic reduction of NH_3 (NH_3-SCR) reaction over the (**a**) fresh and (**b**) hydrothermally aged Cu/SAPO-18 and M-Cu/SAPO-18 samples. Reaction conditions: [NO] = [NH_3] = 500 ppm, [O_2] = 14%, [H_2O] = 5%, N_2 balance, GHSV = 130,000 h^{-1} [149].

Beyond introducing secondary metals, constructing co-existing zeolites represents another innovative approach to optimizing SAPO catalyst performance. While pure-phase Cu/SAPO-34 exhibits excellent hydrothermal stability, its high-temperature SCR activity remains suboptimal. Conversely, pure-phase Cu/SAPO-18 demonstrates distinct reaction characteristics due to its lower Brønsted acid site density and strength, yet its overall performance still holds room for improvement. To simultaneously overcome the limitations of single-phase materials, Zhang et al. [148] innovatively synthesized a Cu/SAPO-18/34 symbiotic zeolite. Characterization and performance testing revealed that this symbiotic structure successfully integrates the advantages of both individual phases, achieving

synergistic enhancement: its NH_3-SCR activity and hydrothermal stability significantly outperform those of either Cu/SAPO-18 or Cu/SAPO-34 alone. Specifically, this catalyst exhibits NO conversion rates exceeding 90% across the 200~575 °C temperature range and maintains over 80% NO conversion even after severe hydrothermal aging at 800 °C. The mechanism behind its enhanced performance can be attributed to: the symbiotic structure provides a higher number and intensity of acid sites, which not only promotes the generation of more active isolated copper ions (Cu^{2+} and Cu^{+}) and suppresses the formation of inert CuO_x clusters, but also facilitates the adsorption and activation of reactant molecules (NH_3 and NO). In situ DRIFTS studies reveal the generation of multiple intermediate species including -NH_2, NH_4^+, NO_3^-, and NO_2^- during the reaction. Unlike Cu/SAPO-34, which follows solely the L-H mechanism, the Cu/SAPO-18/34 co-supported zeolite, similar to Cu/SAPO-18, follows a mixed L-H and E-R reaction mechanism. Due to the lower reaction barrier, the L-H mechanism dominates. This work provides a novel approach for designing and developing a new generation of high-performance SAPO-based SCR catalysts.

In summary, non-mainstream zeolite supports such as SSZ-16, UZM-9, and SAPO-18 demonstrate significant application potential in high-temperature NH_3-SCR systems. This chapter's discussion indicates that these materials typically exhibit unique performance advantages in specific aspects: For instance, SSZ-16's distinctive pore architecture endows Cu species with exceptional sintering resistance and high N_2 selectivity, enabling efficient denitrification across an ultra-wide temperature window (300~700 °C). UZM-9 similarly exhibits broad activity ranges, though its N_2O generation under high loading requires urgent resolution. SAPO-18 modified with rare earth elements like Ce achieves synergistic improvements in both activity and hydrothermal stability, with more in-depth mechanistic studies. However, it must be clearly recognized that these "other" supports still face significant common challenges in transitioning from laboratory research to industrial application. First, their synthesis costs are often higher, with more expensive templates or more complex processes, directly limiting the feasibility of large-scale production. Second, for most materials, their long-term hydrothermal stability has not been systematically and fully evaluated, which is a critical test in the actual operating environment of gas turbines. Finally, relevant research is currently largely confined to ideal laboratory conditions, lacking performance verification under pilot-scale or actual flue gas conditions.

8. Comparison of Catalytic Characteristics and Mechanisms for Fe/Cu-Based Zeolite Catalysts with Doping Modification in High-Temperature NH_3-SCR

To more clearly elucidate the regulatory effects of different metallic elements, Table 3 systematically summarizes the influence of various metal doping on the performance of Fe/Cu-based zeolite catalysts.

Table 3. Effect of different metal doping on the performance of Fe/Cu-Based zeolite catalysts.

Primary Active Metals	Doped Modifying Elements	Reaction Mechanism	Advantages After Doping	Core Limitations	Typical Zeolite Support	References
Fe	—	E-R or L-H	—	Severe oxidation of NH_3 at high temperatures, with poor activity above 600 °C	ZSM-5, Beta, SSZ-13, SAPO-34	[38,39,91–96,100–102,123]

Table 3. *Cont.*

Primary Active Metals	Doped Modifying Elements	Reaction Mechanism	Advantages After Doping	Core Limitations	Typical Zeolite Support	References
Fe	Zr	E-R	Enhance the dispersion of iron species, increase acidic sites, promote the formation of intermediates, and improve hydrothermal stability	The preparation method is complex and may clog the channels	SSZ-13	[110]
	Ce	E-R or L-H	Promote NO_x adsorption and activation, enhancing high-temperature SCR activity and hydrothermal stability	Severe oxidation of NH_3 at high temperatures and poor hydrothermal stability	ZSM-5, Beta	[41,85–87]
	Gd	E-R or L-H	Inhibit the agglomeration of iron species and enhance the stability of the zeolite framework	The high cost of the rare earth element Gd	Beta	[98]
	Ni, W	E-R or L-H	Significantly inhibits the oxidation of NH_3	The preparation method is complex	ZSM-5	[90]
Cu	—	E-R or L-H	—	Poor high-temperature activity	ZSM-5, Beta, SSZ-13, SAPO-34	[104,124–126]
	—	E-R or L-H	—	The preparation method is complex and costly, and it produces the byproduct N_2O	SSZ-16, UZM-9	[132–134]
	Fe	E-R or L-H	Significantly enhanced high-temperature activity	The preparation method is complex	SSZ-13, SAPO-34	[114,128,129]
	Nb	L-H	The formed Nb=O can increase acidity, optimize the species distribution of Cu, and enhance redox capability	The optimal load capacity of Nb is critical, but it comes at a high cost	SSZ-13	[117,118]
	Zn	E-R or L-H	Inhibit Cu^{2+} migration and sintering to enhance hydrothermal stability	Zn may be toxic under certain conditions, and its framework may collapse at extremely high temperatures	SSZ-13	[112]
	Ti	E-R or L-H	Protect the molecular sieve framework to enhance hydrothermal stability	Ti modification is costly and requires post-processing	SSZ-13	[111]
	Ce	E-R and L-H	Enhance high-temperature performance and inhibit backbone hydrolysis	The preparation method is complex	SAPO-18	[145]
	Y	E-R or L-H	Stabilize the molecular sieve framework and protect Brønsted acid sites	The cost of the rare earth element Y is high	SSZ-13	[113]

9. Outlook and Future Research Directions

Despite demonstrating significant potential in high-temperature NH_3-SCR applications, zeolite-based catalysts face substantial challenges in transitioning from laboratory research to commercial gas turbine deployment. Based on the systematic analysis presented in this review, future research must achieve breakthroughs across four dimensions—mechanism understanding, design methodologies, engineering validation, and sustainability—to bridge the gap between fundamental research and industrial demands.

9.1. Deepening Mechanistic Understanding Through Ultra-High-Temperature In Situ Characterization

Currently, research on reaction mechanisms at temperatures above 600 °C remains fragmented, particularly regarding the dynamic evolution of active sites and the competitive mechanisms between primary and secondary reactions. Future studies should leverage advanced in situ/operational characterization techniques to capture real-time structural changes:

For iron-based zeolites (such as Fe/ZSM-5, Fe/SSZ-13), in situ X-ray absorption spectroscopy (XAS) should be employed to track the valence state transition ($Fe^{3+} \leftrightarrow Fe^{2+}$) of iron species and the agglomeration behavior of oligomeric Fe_xO_y clusters under high-temperature (500~700 °C) and high-steam-vapor conditions. This will clarify why isolated Fe^{3+} sites remain stable at 750 °C, while oligomeric clusters readily sinter [38,102].

For copper-based zeolites (e.g., Cu/SSZ-13, Cu/SAPO-34), it is necessary to combine in situ diffuse reflect Fourier transform infrared spectroscopy (DRIFTS) with mass spectrometry (MS) to identify key intermediates (e.g., -NH_2, NO_2^-, NH_4^+) and quantify their conversion rates to clarify whether the reaction at 600 °C primarily follows the L-H mechanism or the E-R mechanism [106,125].

For composite metal modification systems (e.g., Ce-Fe/Beta, Zr-Cu/SSZ-13), in situ electron paramagnetic resonance (EPR) can characterize intermetallic synergistic effects (e.g., Ce^{3+}/Ce^{4+} redox cycling promoting Fe^{3+} dispersion) and their influence on suppressing NH_3 overoxidation [41,110].

9.2. Advancing Rational Catalyst Design Using Density Functional Theory and Machine Learning

Traditional trial-and-error methods are inefficient for optimizing zeolite catalysts; integrating theoretical calculations and artificial intelligence is critical to accelerating development:

Density functional theory (DFT) calculations provide a powerful means to unravel reaction mechanisms and material properties at the atomic scale, offering quantitative insights that can break the reliance on traditional trial-and-error approaches. For instance, the team led by Academician He Hong [150] utilized DFT to elucidate the stabilization mechanism of Yttrium (Y)-modified Cu/SSZ-39 catalysts. Their calculations revealed that Y doping significantly increases the energy barrier for breaking the framework Al-O bonds, thereby effectively suppressing dealumination during hydrothermal aging. To enhance SO_2 tolerance, a research group [151] from Fuzhou University employed DFT computations to investigate ZnO-modified Fe-Cu/SSZ-13. Their study found that SO_2 exhibits an extremely high adsorption energy (−7.62 eV) at the ZnO interface sites, compared to a much lower adsorption energy (−0.65 eV) at the Cu active sites. This indicates a "sacrificial protection" mechanism, where SO_2 molecules are preferentially and strongly chemisorbed at the ZnO sites, effectively shielding the intrinsic Cu active centers. This mechanism, further verified by in situ XAFS and DRIFTS, enables the catalyst to maintain over 90% NO_x conversion under harsh conditions containing 20 ppm SO_2 and 20 vol% H_2O. For Cu/SSZ-13 with CHA topology, European research teams [152] employed the PBE+U functional (with a Hubbard U value of 6 eV for Cu 3d orbitals) combined with Grimme-D3 van der Waals correction. They calculated that the energy barrier for the conversion of Z_2Cu^{2+} to ZCu^+ is 0.82 eV, and the co-adsorption energy of NO + O_2 is 1.27 eV. This confirms that single Cu^+ ions dominate the high-temperature reaction. Furthermore, through transition state search using the Climbing Image Nudged Elastic Band (CI-NEB) method, they verified that the formation of NO_3^- is the rate-determining step, with an activation energy of 0.89 eV. Furthermore, DFT studies on OFF/ERI intergrown zeolites demonstrated that the unique intergrowth interface leads to a substantially higher Cu^{2+} exchange energy (177.3 kJ/mol) compared to that of individual ERI (91.6 kJ/mol) or OFF (76.3 kJ/mol) structures. This

theoretically explains the material's superior ability to stabilize isolated Cu^{2+} ions and its exceptional hydrothermal stability [153].

While DFT unravels atomic-scale mechanisms for diverse zeolite systems, machine learning (ML) complements this by leveraging experimental data to guide practical synthesis. For instance, A representative study by a South Korean research team focused on Beta (BEA) and ZSM-5 (MFI) zeolites [154]. They constructed a database encompassing over 1918 data points from literature. Using a decision tree model, they achieved high prediction accuracy for NO_x conversion (89% for Beta and 85% for ZSM-5). More importantly, the model extracted directly applicable synthesis guidelines. For example, it identified that high low-temperature catalytic activity for Beta zeolite requires "Si/Al $\leq$ 10 and Cu loading $\geq$ 1.0 wt%", whereas for ZSM-5, the condition is "Fe loading between 2.0 and 8.0 wt% and Cu loading at 4.0 wt%". These data-driven guidelines significantly accelerate the targeted design of high-performance catalysts. Future efforts should focus on integrating DFT-derived descriptors into ML models and extending these approaches to more complex multi-component systems, ultimately paving the way for intelligent and precise catalyst design.

9.3. Reducing Synthesis Costs and Advancing Green Manufacturing

The high cost of synthesizing zeolites (especially CHA and AFX types) is the primary bottleneck hindering their industrialization. Therefore, green synthesis represents the primary direction for future development [155–157]. Key focuses include: developing inexpensive alternatives to template agents [158,159], establishing efficient recovery processes for template agents [160,161], and promoting template-free seed-directed synthesis methods [162,163]. Simultaneously, there is an urgent need to establish efficient spent catalyst recycling systems [164]. This involves recovering precious metals through mild leaching techniques (e.g., chelating agents) and developing direct regeneration technologies (e.g., temperature-controlled calcination) to restore catalyst activity. Building a closed-loop material lifecycle—"design-preparation-use-recycling"—is essential not only for economic viability but also aligns with green chemistry principles.

9.4. Verification of Catalyst Performance Under Actual Gas Turbine Operating Conditions

The ideal testing conditions in laboratories differ significantly from the actual operating environment of gas turbines. Future testing must involve endurance tests lasting hundreds or even thousands of hours under complex flue gas conditions characterized by high water vapor content (10~15% H_2O), wide temperature fluctuations (500~700 °C), and trace amounts of SO_2. This represents not only a necessary step in screening final catalyst candidates but also a critical approach to uncovering actual deactivation mechanisms and optimizing regeneration strategies. Ultimately, pilot-scale demonstrations must be actively advanced. Collaboration with industry is essential to validate mechanical strength, pressure drop, and thermal expansion compatibility within real systems—the final hurdle in assessing industrial viability.

For the purpose of facilitating intuitive comparison and summary, the key characteristics, performance metrics, and application potential of the various zeolite catalysts discussed above are systematically summarized in Table 4.

Table 4. Comprehensive comparison of zeolite-supported high-temperature NH_3-SCR catalysts.

Zeolite Type (Topology)	Active Metal	Denitrification Activity	Hydrothermal Stability	Key Advantages	Main Limitations	Synthesis Cost	Industrial Potential
ZSM-5 (MFI)	Fe Ce, Fe W, Zr Sm, W, Zr Fe, Ni, W	(425~680 °C) > 80% (370~600 °C) > 90% (350~630 °C) > 90% (380~640 °C) > 90% (480~750 °C) > 90%	Low Excellent Moderate Moderate Excellent	Low cost, tunable acidity, mature synthesis	Severe oxidation of NH_3 at high temperatures	Low	Medium (for mid-temperature, cost-sensitive scenarios)
Beta (BEA)	Fe Ce, Fe Gd, Fe	(310~600 °C) > 90% (311~683 °C) > 80% (450~600 °C) > 90%	Moderate Excellent Excellent	3D large pores, favorable mass transfer, high surface area	Structural defects, prone to dealumination at high temperatures	Medium	Medium (requires enhanced high-temp stability)
SSZ-13 (CHA)	Cu Zr, Fe Ti, Cu Zn, Cu Fe, Cu Nb, Cu	(200~680 °C) > 90% (430~575 °C) > 90% (250~640 °C) > 90% (200~600 °C) > 90% (200~625 °C) > 90% (200~625 °C) > 90%	Excellent	Outstanding hydrothermal stability, superior shape selectivity	Expensive template, high synthesis cost	High	High (Top candidate for high-temperature use, pending cost reduction)
SAPO-34 (CHA)	Cu Fe, Cu	(300~670 °C) > 90% (250~600 °C) > 90%	Good Good	Good hydrothermal stability, mild acidity suppresses NH_3 oxidation	Activity decline at very high temperatures, complex synthesis control	Medium-High	Medium-High (A viable alternative to SSZ-13)
SSZ-16 (AFX)	Cu	(300~670 °C) > 90%	Good	Ultra-wide temperature window, high N_2 selectivity	Expensive template, potential framework collapse at very high temperature	High	Medium (Potential for ultra-wide temperature scenarios)
UZM-9 (LTA)	Cu	(250~700 °C) > 90%	Good	Broad activity window, seed-assisted synthesis possible	Increased N_2O byproduct formation at high Cu loadings	Medium	Medium (require solving N_2O selectivity issue)
SAPO-18 (AEI)	Ce, Cu	(200~600 °C) > 90%	Good	High N_2 selectivity	Lower Brønsted acidity than SAPO-34	Medium-High	Medium-High (require solving low-cost synthetic routes issue)

10. Conclusions

This review systematically summarizes research progress on zeolite-based catalysts in high-temperature NH_3-SCR applications, aiming to address challenges faced by commercial V_2O_5-WO_3/TiO_2 catalysts in gas turbine high-temperature flue gases. Based on the detailed discussion above and the comprehensive comparison in Table 1, the following core conclusions can be drawn:

The framework topology of zeolites fundamentally determines their performance limits and application scenarios. ZSM-5 (MFI) and Beta (BEA) exhibit advantages in mass transfer due to their channel structures, but their potential for long-term high-temperature (>600 °C) operation is limited by framework stability. In contrast, the cage-like structures of SSZ-13/SAPO-34 (CHA) and its analogues (e.g., SSZ-16/AFX) confer exceptional hydrothermal stability, making them the most promising candidates for high-temperature gas turbine denitration—though their synthesis costs pose a major challenge.

Precision engineering of active metals and modifiers is crucial for achieving high performance. This review demonstrates that isolated Fe^{3+} sites serve as highly efficient centers driving activity at elevated temperatures (600~700 °C), while Cu^{2+} species excel in the medium-to-low temperature range. More importantly, the incorporation of modifiers

such as rare earth elements (Ce, Gd, Y) and transition metals (Zr, Nb) significantly enhances catalyst performance by modulating acidity, stabilizing the framework, and generating synergistic effects. This broadens the temperature window and improves durability.

To translate these scientific insights into industrial reality, future research and development should adopt a prioritized approach. In the short term, priority should be given to the development of composite systems, such as Cu/SSZ-13 modified with Fe or other metals. These catalysts already demonstrate a broad temperature window and excellent hydrothermal stability, and further optimization could yield commercially viable solutions in the near future. For the medium to long term, the focus should shift towards overcoming the primary bottleneck of the most promising yet expensive materials—specifically, achieving a breakthrough in the green synthesis of AFX-type zeolites (e.g., SSZ-16). Success in developing low-cost, template-free, or recyclable template synthesis routes for these top-tier supports would fundamentally enhance the economic feasibility and sustainability of next-generation high-temperature SCR technologies.

In summary, the successful commercialization of zeolite-based high-temperature SCR catalysts is not achieved through breakthroughs in a single performance metric, but rather through a systematic engineering approach involving multi-objective optimization of "structure-performance-cost." Future development hinges on synergistic innovation across four domains: mechanism research, rational design, green manufacturing processes, and engineering validation. Through sustained interdisciplinary efforts, zeolite catalysts hold promise as core technological solutions for clean and efficient gas turbine operation, poised to play a pivotal role in the global energy transition.

Author Contributions: Writing—original draft preparation, X.M.; writing—review and editing, X.M., X.B. and Y.B.; data curation, M.Z., Y.H. and J.W.; supervision, Y.B.; project administration, X.B. and Y.B.; funding acquisition, X.B. All authors have read and agreed to the published version of the manuscript.

Funding: This research received no external funding.

Data Availability Statement: Data sharing is not applicable.

Conflicts of Interest: The authors declare no conflicts of interest.

References

1. Gülen, S.C.; Curtis, M. Gas Turbine's Role in Energy Transition. *J. Eng. Gas Turbines Power* **2024**, *146*, 101008. [CrossRef]
2. Banihabib, R.; Assadi, M. The Role of Micro Gas Turbines in Energy Transition. *Energies* **2022**, *15*, 8084. [CrossRef]
3. Genc, T.S. Energy Transition and the role of new natural gas turbines for power production: The case of GT11N2 M generators. *Energy Econ.* **2024**, *131*, 107412. [CrossRef]
4. Li, S.; Zhang, G.; Wu, Y. Advanced combustion technologies for future gas turbines. *J. Tsinghua Univ. Sci. Technol.* **2021**, *61*, 1423–1437.
5. Liu, Z.; Yao, J.; Zhuang, K.; Yu, L.; Zhou, K. Comparison of Characteristics of SCR-DeNO$_x$ Catalyst for Gas-Turbine Units and Coal-Fired Units. *Electr. Power* **2021**, *54*, 145–152.
6. Xue, H.; Yuan, J.; Wu, M.; Gu, Y.; Ding, D.; Zhang, L. Current Status of Nitrogen Oxide Emissions from Gas Turbine Units and Suggestions for Standard Revision. *Energy Environ.* **2022**, *4*, 90–92. [CrossRef]
7. Qing, M.; Lei, S.; Kong, F.; Liu, L.; Zhang, W.; Wang, L.; Guo, T.; Su, S.; Hu, S.; Wang, Y.; et al. Analysis of ammonium bisulfate/sulfate generation and deposition characteristics as the by-product of SCR in coal-fired flue gas. *Fuel* **2022**, *313*, 122790. [CrossRef]
8. Ma, S.; Guo, M.; Song, H.; Chen, G.; Yang, J.; Zang, B.; Li, Z. Formation mechanism and influencing factors of ammonium bisulfate during the selective catalytic reduction process. *Therm. Power Gener.* **2014**, *43*, 75–78+86.
9. Jiang, Y.; Gao, X.; Wu, W.; Zhang, Y. Review of the Deactivation of Selective Catalytic Reduction DeNO$_x$ Catalysts. *Proc. CSEE* **2013**, *33*, 18–31+13.

10. Chapman, D.M. Behavior of titania-supported vanadia and tungsta SCR catalysts at high temperatures in reactant streams: Tungsten and vanadium oxide and hydroxide vapor pressure reduction by surficial stabilization. *Appl. Catal. A-Gen.* **2011**, *392*, 143–150. [CrossRef]
11. Hanaor, D.A.H.; Sorrell, C.C. Review of the anatase to rutile phase transformation. *J. Mater. Sci.* **2011**, *46*, 855–874. [CrossRef]
12. Rasmussen, S.B.; Abrams, B.L. Fundamental chemistry of V-SCR catalysts at elevated temperatures. *Catal. Today* **2017**, *297*, 60–63. [CrossRef]
13. Busca, G.; Lietti, L.; Ramis, G.; Berti, F. Chemical and mechanistic aspects of the selective catalytic reduction of NO_x by ammonia over oxide catalysts: A review. *Appl. Catal. B Environ.* **1998**, *18*, 1–36. [CrossRef]
14. Lu, Q.; Wu, Y.; Xu, M.; Qu, Y.; Wang, H.; Pei, X.; Ouyang, H. Progress in the Development of SCR Denitration Catalysts with Resistance of High-temperature Deactivation. *Mater. Rep.* **2022**, *36*, 68–76.
15. Jin, P.; Chen, Z.; Jin, R.; Chen, Y.; Liu, Z.; Zhuang, K.; Yu, L.; Sheng, Z. Study on deNO_x Performance of Cu-based Zeolites Catalyst in the Wide Temperature NH_3-SCR. *Saf. Environ. Eng.* **2023**, *30*, 233–240.
16. Wang, Y.; Tang, T.; Zhou, Q.; Xu, L.; Tang, C. Research progress in high-temperature SCR denitration: From catalyst innovations to reaction mechanism exploration. *Electr. Power Technol. Environ. Prot.* **2025**, *41*, 343–356.
17. Sa, A.; Zubaidy, S. Gas turbine performance at varying ambient temperature. *Appl. Therm. Eng.* **2011**, *31*, 2735–2739. [CrossRef]
18. Chen, Q. Treatment of Large Exhaust Temperature Deviation of Siemens F-Class Gas Turbine in a Factory. *Power Energy* **2017**, *38*, 354–357.
19. Kurata, O.; Iki, N.; Matsunuma, T.; Inoue, T.; Tsujimura, T.; Furutani, H.; Kobayashi, H.; Hayakawa, A. Performances and emission characteristics of NH_3–air and NH_3 single bond CH_4–air combustion gas-turbine power generations. *Proc. Combust. Inst.* **2017**, *36*, 3351–3359. [CrossRef]
20. Luca, L.; Isabella, N.; Gianguido, R.; Lorenzo, D.; Guido, B.; Elio, G.; Pio, F.; Fiorenzo, B. Characterization and Reactivity of V_2O_5–MoO_3/TiO_2 De-NO_x SCR Catalysts. *J. Catal.* **1999**, *187*, 419–435.
21. Casagrandea, L.; Liettia, L.; Novaa, I.; Forzattia, P.; Baiker, A. SCR of NO by NH_3 over TiO_2-supported V_2O_5–MoO_3 catalysts: Reactivity and redox behavior. *Appl. Catal. B Environ.* **1999**, *22*, 63–77. [CrossRef]
22. Zhang, Q.-M.; Song, C.-L.; Lv, G.; Bin, F.; Pang, H.-T.; Song, J.-O. Effect of metal oxide partial substitution of V_2O_5 in V_2O_5–WO_3/TiO_2 on selective catalytic reduction of NO with NH_3. *J. Ind. Eng. Chem.* **2015**, *24*, 79–86. [CrossRef]
23. Chen, M.; Jin, Q.; Tao, X.; Pan, Y.; Gu, S.; Shen, Y. Novel W-Zr-O_x/TiO_2 catalyst for selective catalytic reduction of NO by NH_3 at high temperature. *Catal. Today* **2020**, *358*, 254–262. [CrossRef]
24. Bian, X.; Xu, Q.; Cai, M.; Cen, P.; Wu, W. The SCR reaction and mechanism of a silicic acid modified Ce-W/TiO_2 catalyst. *New J. Chem.* **2022**, *46*, 15596–15604. [CrossRef]
25. Wachs, I.E. Raman and IR studies of surface metal oxide species on oxide supports: Supported metal oxide catalysts. *Catal. Today* **1996**, *27*, 437–455. [CrossRef]
26. Madia, G.; Elsener, M.; Koebel, M.; Raimondi, F.; Wokaun, A. Thermal stability of vanadia-tungsta-titania catalysts in the SCR process. *Appl. Catal. B Environ.* **2002**, *39*, 181–190. [CrossRef]
27. Liu, X.; Wu, X.; Xu, T.; Weng, D.; Si, Z.; Ran, R. Effects of silica additive on the NH_3-SCR activity and thermal stability of a V_2O_5/WO_3-TiO_2 catalyst. *Chin. J. Catal.* **2016**, *37*, 1340–1346. [CrossRef]
28. Huang, Y.; Xu, J.; Ling, H.; Liu, W.; Jiao, F. Deactivation Mechanism of Spent TiO_2-Based Selective Catalytic Reduction (SCR) Catalysts and State-of-the-Art Recycling Technologies. *Langmuir* **2024**, *40*, 26371–26386. [CrossRef]
29. Yang, G.; Zhao, H.; Luo, X.; Shi, K.; Zhao, H.; Wang, W.; Chen, Q.; Fan, H.; Wu, T. Promotion effect and mechanism of the addition of Mo on the enhanced low temperature SCR of NO_x by NH_3 over MnO_x/γ-Al_2O_3 catalysts. *Appl. Catal. B Environ.* **2019**, *245*, 743–752. [CrossRef]
30. Shi, A.; Wang, X.; Yu, T.; Shen, M. The effect of zirconia additive on the activity and structure stability of V_2O_5/WO_3-TiO_2 ammonia SCR catalysts. *Appl. Catal. B Environ.* **2011**, *106*, 359–369. [CrossRef]
31. Si, W.; Liu, H.; Yan, T.; Wang, H.; Fan, C.; Xiong, S.; Zhao, Z.; Peng, Y.; Chen, J.; Li, J. Sn-doped rutile TiO_2 for vanadyl catalysts: Improvements on activity and stability in SCR reaction. *Appl. Catal. B Environ.* **2020**, *269*, 118797. [CrossRef]
32. Kwon, D.W.; Lee, S.; Kim, J.; Lee, K.-Y.; Ha, H.P. Influence of support composition on enhancing the performance of Ce-V on TiO_2 comprised tungsten-silica for NH_3-SCR. *Catal. Today* **2021**, *359*, 112–123. [CrossRef]
33. Liu, Q.; Bian, C.; Ming, S.; Guo, L.; Zhang, S.; Pang, L.; Liu, P.; Chen, Z.; Li, T. The opportunities and challenges of iron-zeolite as NH_3-SCR catalyst in purification of vehicle exhaust. *Appl. Catal. A-Gen.* **2020**, *607*, 117865. [CrossRef]
34. Zhang, W.; Chen, J.; Guo, L.; Zheng, W.; Wang, G.; Zheng, S.; Wu, X. Research progress on NH_3-SCR mechanism of metal-supported zeolite catalysts. *J. Fuel Chem. Technol.* **2021**, *49*, 1294–1315. [CrossRef]
35. Yuan, Y.; Guan, B.; Chen, J.; Zhuang, Z.; Zheng, C.; Zhou, J.; Su, T.; Zhu, C.; Guo, J.; Dang, H.; et al. Research status and outlook of molecular sieve NH_3-SCR catalysts. *Mol. Catal.* **2024**, *554*, 113846. [CrossRef]
36. Simancas, R.; Chokkalingam, A.; Elangovan, S.P.; Liu, Z.; Sano, T.; Iyoki, K.; Wakihara, T.; Okubo, T. Recent progress in the improvement of hydrothermal stability of zeolites. *Chem. Sci.* **2021**, *12*, 7677–7695. [CrossRef]

37. Breck, D.W. *Zeolite Molecular Sieves: Structure, Chemistry, and Use*; John Wiley & Sons: New York, NY, USA, 1974.
38. Wang, P.; Yu, D.; Zhang, L.; Ren, Y.; Jin, M.; Lei, L. Evolution mechanism of NO_x in NH_3-SCR reaction over Fe-ZSM-5 catalyst: Species-performance relationships. *Appl. Catal. A-Gen.* **2020**, *607*, 117806. [CrossRef]
39. Yu, D.; Wang, P.; Li, X.; Zhao, H.; Lv, X. Study on the role of Fe species and acid sites in NH_3-SCR over the Fe-based zeolites. *Fuel* **2023**, *336*, 126759. [CrossRef]
40. Liu, J.; Du, Y.; Liu, J.; Zhao, Z.; Cheng, K.; Chen, Y.; Wei, Y.; Song, W.; Zhang, X. Design of MoFe/Beta@CeO_2 catalysts with a core−shell structure and their catalytic performances for the selective catalytic reduction of NO with NH_3. *Appl. Catal. B Environ.* **2017**, *203*, 704–714. [CrossRef]
41. Zhang, Y.; Wang, P.; Zhao, H.; Lyu, X.; Lei, L.; Zhang, L. The promoting mechanism of Ce on the hydrothermal stability of Fe-Beta catalyst for NH_3-SCR reaction. *Microporous Mesoporous Mater.* **2022**, *338*, 111937. [CrossRef]
42. Wang, Y.; Shi, X.; Shan, Y.; Du, J.; Liu, K.; He, H. Hydrothermal Stability Enhancement of Al-Rich Cu-SSZ-13 for NH_3 Selective Catalytic Reduction Reaction by Ion Exchange with Cerium and Samarium. *Ind. Eng. Chem. Res.* **2020**, *59*, 6416–6423. [CrossRef]
43. Wang, J.; Peng, Z.; Chen, Y.; Bao, W.; Chang, L.; Feng, G. In-situ hydrothermal synthesis of Cu-SSZ-13/cordierite for the catalytic removal of NO_x from diesel vehicles by NH_3. *Chem. Eng. J.* **2015**, *263*, 9–19. [CrossRef]
44. Zhang, T.; Qiu, F.; Li, J. Design and synthesis of core-shell structured meso-Cu-SSZ-13@mesoporous aluminosilicate catalyst for SCR of NO with NH_3: Enhancement of activity, hydrothermal stability and propene poisoning resistance. *Appl. Catal. B Environ.* **2016**, *195*, 48–58. [CrossRef]
45. Xu, H.; Lin, C.; Lin, Q.; Feng, X.; Zhang, Z.; Wang, Y.; Chen, Y. Grain size effect on the high-temperature hydrothermal stability of Cu/SAPO-34 catalysts for NH_3-SCR. *J. Environ. Chem. Eng.* **2020**, *8*, 104559. [CrossRef]
46. Jabłońska, M. Recent progress in the selective catalytic reduction of NO with NH3 on Cu-SAPO-34 catalysts. *Mol. Catal.* **2022**, *518*, 112111. [CrossRef]
47. Gao, F.; Walter, E.D.; Karp, E.M.; Luo, J.; Tonkyn, R.G.; Kwak, J.H.; Szanyi, J.; Peden, C.H.F. Structure–activity relationships in NH_3-SCR over Cu-SSZ-13 as probed by reaction kinetics and EPR studies. *J. Catal.* **2013**, *300*, 20–29. [CrossRef]
48. Ruggeri, M.P.; Nova, I.; Tronconi, E.; Collier, J.E.; York, A.P.E. Structure–Activity Relationship of Different Cu–Zeolite Catalysts for NH_3-SCR. *Top. Catal.* **2016**, *59*, 875–881. [CrossRef]
49. Huang, X.; Zhang, G.; Lu, G.; Tang, Z. Recent Progress on Establishing Structure–Activity Relationship of Catalysts for Selective Catalytic Reduction (SCR) of NO_x with NH_3. *Catal. Surv. Asia* **2017**, *22*, 1–19. [CrossRef]
50. Yang, Y.; Liu, J.; Liu, F.; Wang, Z.; Ding, J.; Huang, H. Reaction mechanism for NH_3-SCR of NO_x over $CuMn_2O_4$ catalyst. *Chem. Eng. J.* **2019**, *361*, 578–587. [CrossRef]
51. Shi, Z.; Peng, Q.; Jiaqiang, E.; Xie, B.; Wei, J.; Yin, R.; Fu, G. Mechanism, performance and modification methods for NH_3-SCR catalysts: A review. *Fuel* **2023**, *331*, 125885. [CrossRef]
52. Sun, Q.; Wang, N.; Yu, J. Advances in Catalytic Applications of Zeolite-Supported Metal Catalysts. *Adv. Mater.* **2021**, *33*, 2104442. [CrossRef] [PubMed]
53. Mohan, S.; Dinesha, P.; Kumar, S. NOx reduction behaviour in copper zeolite catalysts for ammonia SCR systems: A review. *Chem. Eng. J.* **2020**, *384*, 123253. [CrossRef]
54. Damma, D.; Ettireddy, P.; Reddy, B.; Smirniotis, P. A Review of Low Temperature NH_3-SCR for Removal of NOx. *Catalysts* **2019**, *9*, 349. [CrossRef]
55. Elkaee, S.; Phule, A.D.; Yang, J.H. Advancements in (SCR) technologies for NOx reduction: A comprehensive review of reducing agents. *Process Saf. Environ. Prot.* **2024**, *184*, 854–880. [CrossRef]
56. Zhang, R.; Liu, N.; Lei, Z.; Chen, B. Selective Transformation of Various Nitrogen-Containing Exhaust Gases toward N_2 over Zeolite Catalysts. *Chem. Rev.* **2016**, *116*, 3658–3721. [CrossRef]
57. Liu, Z.G.; Ottinger, N.A.; Cremeens, C.M. Vanadium and tungsten release from V-based selective catalytic reduction diesel aftertreatment. *Atmos. Environ.* **2015**, *104*, 154–161. [CrossRef]
58. Corma, A. From Microporous to Mesoporous Molecular Sieve Materials and Their Use in Catalysis. *Chem. Rev.* **1997**, *97*, 2373–2420. [CrossRef]
59. International Zeolite Association. Available online: https://www.iza-online.org/ (accessed on 9 September 2025).
60. Valentin, V.; Mintova, S. Layer-by-layer preparation of zeolite coatings of nanosized crystals. *Microporous Mesoporous Mater.* **2001**, *43*, 41–49.
61. Tang, G.; Li, Y.; Wang, Y.; Chai, Y.; Liu, C. A review on the synthesis, structural modification and application of two-dimensional MFI zeolite. *J. Porous Mater.* **2022**, *29*, 1649–1666. [CrossRef]
62. Wang, H.; Xu, R.; Jin, Y.; Zhang, R. Zeolite structure effects on Cu active center, SCR performance and stability of Cu-zeolite catalysts. *Catal. Today* **2019**, *327*, 295–307. [CrossRef]
63. Newsam, J.M.; Treacy, M.M.; Koetsier, W.T.; Gruyter, C.D. Structural characterization of zeolite beta. *Proc. R. Soc. Lond A* **1988**, *420*, 375–405.

64. Zhang, J.; Shan, Y.; Zhang, L.; Du, J.; He, H.; Han, S.; Lei, C.; Wang, S.; Fan, W.; Feng, Z.; et al. Importance of controllable Al sites in CHA framework by crystallization pathways for NH_3-SCR reaction. *Appl. Catal. B Environ.* **2020**, *277*, 119193. [CrossRef]
65. Chen, L.; Janssens, T.V.W.; Vennestrøm, P.N.R.; Jansson, J.; Skoglundh, M.; Grönbeck, H. A Complete Multisite Reaction Mechanism for Low-Temperature NH_3-SCR over Cu-CHA. *ACS Catal.* **2020**, *10*, 5646–5656. [CrossRef]
66. Pu, X.; Liu, X.; Wang, Y.; Jia, Y.; Zhang, P. Research progress on Cu-SAPO-34 denitration catalyst Cu-SAPO-34. *Ind. Catal.* **2023**, *31*, 12–17.
67. Zones, S.I. Conversion of Faujasites to High-silica Chabazite SSZ-13 in the Presence of *N*,*N*,*N*-Trimethyl-1-adamantammonium Iodide. *J. Chem. Soc. Faraday Trans.* **1991**, *87*, 3709–3716. [CrossRef]
68. Khana, N.; Yooa, D.; Bhadraa, B.; Junb, J.; Kimb, T.; Kimb, C.; Jhunga, S. Preparation of SSZ-13 zeolites from beta zeolite and their application in the conversion of ethylene to propylene. *Chem. Eng. J.* **2019**, *377*, 119546. [CrossRef]
69. Xie, L.; Liu, F.; Ren, L.; Shi, X.; Xiao, F.; He, H. Excellent Performance of One-Pot Synthesized Cu-SSZ-13 Catalyst for the Selective Catalytic Reduction of NO_x with NH_3. *Environ. Sci. Technol.* **2014**, *48*, 566–572. [CrossRef] [PubMed]
70. Fickel, D.W.; Lobo, R.F. Copper Coordination in Cu-SSZ-13 and Cu-SSZ-16 Investigated by Variable-Temperature XRD. *J. Phys. Chem. C* **2010**, *114*, 1633–1640. [CrossRef]
71. Tsunoji, N.; Tsuchiya, K.; Nakazawa, N.; Inagaki, S.; Kubota, Y.; Nishitoba, T.; Yokoi, T.; Ohnishi, T.; Ogura, M.; Sadakane, M.; et al. Multiple templating strategy for the control of aluminum and phosphorus distributions in AFX zeolite. *Microporous Mesoporous Mater.* **2021**, *321*, 111124. [CrossRef]
72. Qi, X.; Wang, Y.; Liu, C.; Liu, Q. The Challenges and Comprehensive Evolution of Cu-Based Zeolite Catalysts for SCR Systems in Diesel Vehicles: A Review. *Catal. Surv. Asia* **2022**, *27*, 181–206. [CrossRef]
73. Martínez-Franco, R.; Moliner, M.; Corma, A. Direct synthesis design of Cu-SAPO-18, a very efficient catalyst for the SCR of NO_x. *J. Catal.* **2014**, *319*, 36–43. [CrossRef]
74. Moliner, M.; Franch, C.; Palomares, E.; Grill, M.; Corma, A. Cu–SSZ-39, an active and hydrothermally stable catalyst for the selective catalytic reduction of NO_x. *Chem. Commun.* **2012**, *48*, 8264–8266. [CrossRef]
75. Ryu, T.; Kim, H.; Hong, S.B. Nature of active sites in Cu-LTA NH_3-SCR catalysts: A comparative study with Cu-SSZ-13. *Appl. Catal. B Environ.* **2019**, *245*, 513–521. [CrossRef]
76. Han, L.; Cai, S.; Gao, M.; Hasegawa, J.-Y.; Wang, P.; Zhang, J.; Shi, L.; Zhang, D. Selective Catalytic Reduction of NO_x with NH_3 by Using Novel Catalysts: State of the Art and Future Prospects. *Chem. Rev.* **2019**, *119*, 10916–10976. [CrossRef]
77. Shan, Y.; Du, J.; Zhang, Y.; Shan, W.; Shi, X.; Yu, Y.; Zhang, R.; Meng, X.; Xiao, F.-S.; He, H. Selective catalytic reduction of NO_x with NH_3: Opportunities and challenges of Cu-based small-pore zeolites. *Natl. Sci. Rev.* **2021**, *8*, nwab010. [CrossRef]
78. Long, R.; Yang, R. Catalytic Performance of Fe–ZSM-5 Catalysts for Selective Catalytic Reduction of Nitric Oxide by Ammonia. *J. Catal.* **1999**, *188*, 332–339. [CrossRef]
79. Ma, A.-Z.; Grünert, W. Selective catalytic reduction of NO by ammonia over Fe-ZSM-5 catalysts. *Chem. Commun.* **1999**, *1999*, 71–72. [CrossRef]
80. Long, R.Q.; Yang, R.T. Reaction Mechanism of Selective Catalytic Reduction of NO with NH_3 over Fe-ZSM-5 Catalyst. *J. Catal.* **2002**, *207*, 224–231. [CrossRef]
81. Brandenberger, S.; Kröcher, O.; Tissler, A.; Althoff, R. The determination of the activities of different iron species in Fe-ZSM-5 for SCR of NO by NH_3. *Appl. Catal. B Environ.* **2010**, *95*, 348–357. [CrossRef]
82. Qi, G.; Wang, Y.; Yang, R.T. Selective Catalytic Reduction of Nitric Oxide with Ammonia over ZSM-5 Based Catalysts for Diesel Engine Applications. *Catal. Lett.* **2007**, *121*, 111–117. [CrossRef]
83. Shi, X.; Liu, F.; Shan, W.; He, H. Selective Catalytic Reduction of NO_x with NH_3 over Fe-ZSM-5 Catalysts. In *Abstracts of Session 2, 28th Annual Meeting of the Chinese Chemical Society*; Chinese Chemical Society: Beijing, China; Available online: https://kns.cnki.net/kcms2/article/abstract?v=ZHE1803t14tVnDFTXmxRBogUw2nC36yJPbxJy0j5GvviUqAXIURKp5CC6DtoenvICuHu8VY_l5GC6OSYTiT61GJu1ir7a8zMhH6NlKhuH1AYL1mwKBOFX1ib_4ajO8saDhjNfDleYkU8evPgcyTnRIQQIUPjC96wTt6fYvlw_EVB-ygjgAMKTw==&uniplatform=NZKPT&language=CHS (accessed on 3 November 2025).
84. Shi, X.; Liu, F.; Shan, W.; He, H. Hydrothermal Deactivation of Fe-ZSM-5 Prepared by Different Methods for the Selective Catalytic Reduction of NO_x with NH_3. *Chin. J. Catal.* **2012**, *33*, 454–464. [CrossRef]
85. Chen, Y.; Lin, T.; Liu, Z.; Cao, Y.; Gong, M.; Chen, Y. Influence of Ce and La modified Fe-ZSM-5 catalyst on NH_3-SCR reaction property. *Chem. Res. Appl.* **2013**, *25*, 1065–1068.
86. Long, R.Q.; Yang, R.T. Superior Fe-ZSM-5 Catalyst for Selective Catalytic Reduction of Nitric Oxide by Ammonia. *J. Am. Chem. Soc.* **1999**, *121*, 5595–5596. [CrossRef]
87. Wang, D.; Wang, L.; Gao, G.; Xue, X.; Wu, P.; Zhang, Y. Performance of selective catalytic reduction of NO_x over Ce-Fe/ZSM-5 catalysts for denitrification of gas turbines. *Chin. J. Process Eng.* **2020**, *20*, 718–727.
88. Feng, S.; Li, Z.; Shen, B.; Yuan, P.; Wang, B.; Liu, L.; Wang, Z.; Ma, J.; Kong, W. High activity of NH_3-SCR at high temperature over W-Zr/ZSM-5 in the exhaust gas of diesel engine. *Fuel* **2022**, *323*, 124337. [CrossRef]

89. Feng, S.; Kong, W.; Wang, Y.; Xing, Y.; Wang, Z.; Ma, J.; Shen, B.; Chen, L.; Yang, J.; Li, Z.; et al. Mechanistic investigation of Sm doping effects on SO_2 resistance of W-Zr-ZSM-5 catalyst for NH_3-SCR. *Fuel* **2023**, *353*, 129139. [CrossRef]
90. Liu, H.; You, C.; Wang, H. Experimental and Density Functional Theory Studies on the Zeolite-Based Fe–Ni–W Trimetallic Catalyst for High-Temperature NO_x Selective Catalytic Reduction: Identification of Active Sites Suppressing Ammonia Over-oxidation. *ACS Catal.* **2021**, *11*, 1189–1201. [CrossRef]
91. Liu, Z.; Millington, P.J.; Bailie, J.E.; Rajaram, R.R.; Anderson, J.A. A comparative study of the role of the support on the behaviour of iron based ammonia SCR catalysts. *Microporous Mesoporous Mater.* **2007**, *104*, 159–170. [CrossRef]
92. Frey, A.M.; Mert, S.; Due-Hansen, J.; Fehrmann, R.; Christensen, C.H. Fe-BEA Zeolite Catalysts for NH_3-SCR of NO_x. *Catal. Lett.* **2009**, *130*, 1–8. [CrossRef]
93. Zhu, Y.; Chen, B.; Zhao, R.; Zhao, Q.; Gies, H.; Xiao, F.-S.; De Vos, D.; Yokoi, T.; Bao, X.; Kolb, U.; et al. Fe-doped Beta zeolite from organotemplate-free synthesis for NH_3-SCR of NO_x. *Catal. Sci. Technol.* **2016**, *6*, 6581–6592. [CrossRef]
94. Ma, L.; Chang, H.; Yang, S.; Chen, L.; Fu, L.; Li, J. Relations between iron sites and performance of Fe/HBEA catalysts prepared by two different methods for NH_3-SCR. *Chem. Eng. J.* **2012**, *209*, 652–660. [CrossRef]
95. Liu, H.; Wang, J.; Yu, T.; Fan, S.; Shen, M. The role of various iron species in Fe-β catalysts with low iron loadings for NH_3-SCR. *Catal. Sci. Technol.* **2014**, *4*, 1350–1356. [CrossRef]
96. Shi, J.; Zhang, Y.; Zhang, Z.; Fan, Z.; Chen, M.; Zhang, Z.; Shangguan, W. Water promotion mechanism on the NH_3-SCR over Fe-BEA catalyst. *Catal. Commun.* **2018**, *115*, 59–63. [CrossRef]
97. Klukowski, D.; Balle, P.; Geiger, B.; Wagloehner, S.; Kureti, S.; Kimmerle, B.; Baiker, A.; Grunwaldt, J.D. On the mechanism of the SCR reaction on Fe/HBEA zeolite. *Appl. Catal. B Environ.* **2009**, *93*, 185–193. [CrossRef]
98. Sultana, A.; Fujitani, T.; Iki, N. Development and validation of rare earth modified Fe-BEA SCR catalyst for mitigation of NO_x from NH_3 gas turbine. *Clean. Mater.* **2022**, *4*, 100096. [CrossRef]
99. Kielland, B. Individual Activity Coefficients of Ions in Aqueous Solutions. *J. Am. Chem. Soc.* **1937**, *59*, 1675–1678. [CrossRef]
100. Gao, F.; Kollár, M.; Kukkadapu, R.K.; Washton, N.M.; Wang, Y.; Szanyi, J.; Peden, C.H.F. Fe/SSZ-13 as an NH_3-SCR catalyst: A reaction kinetics and FTIR/Mössbauer spectroscopic study. *Appl. Catal. B Environ.* **2015**, *164*, 407–419. [CrossRef]
101. Gao, F.; Zheng, Y.; Kukkadapu, R.K.; Wang, Y.; Walter, E.D.; Schwenzer, B.; Szanyi, J.; Peden, C.H.F. Iron Loading Effects in Fe/SSZ-13 NH_3-SCR Catalysts: Nature of the Fe Ions and Structure–Function Relationships. *ACS Catal.* **2016**, *6*, 2939–2954. [CrossRef]
102. Liu, Q.; Bian, C.; Jin, Y.; Pang, L.; Chen, Z.; Li, T. Influence of calcination temperature on the evolution of Fe species over Fe-SSZ-13 catalyst for the NH_3-SCR of NO. *Catal. Today* **2022**, *388–389*, 158–167. [CrossRef]
103. Chen, M.; Bi, J.; Liu, C.; Ren, S.-B. Enhancing performance of Fe-SSZ-13 and Cu-Fe-SSZ-13 zeolites for selective catalytic reduction reaction via post-treatment method. *Mater. Lett.* **2023**, *349*, 134872. [CrossRef]
104. Kwak, J.H.; Tonkyn, R.G.; Kim, D.H.; Szanyi, J.; Peden, C.H.F. Excellent activity and selectivity of Cu-SSZ-13 in the selective catalytic reduction of NO_x with NH_3. *J. Catal.* **2010**, *275*, 187–190. [CrossRef]
105. Han, M.-J.; Jiao, Y.-L.; Zhou, C.-H.; Guo, Y.-L.; Guo, Y.; Lu, G.-Z.; Wang, L.; Zhan, W.-C. Catalytic activity of Cu–SSZ-13 prepared with different methods for NH_3-SCR reaction. *Rare Met.* **2018**, *38*, 210–220. [CrossRef]
106. Wang, X.; Xu, Y.; Qin, M.; Zhao, Z.; Fan, X.; Li, Q. Insight into the effects of Cu^{2+} ions and CuO species in Cu-SSZ-13 catalysts for selective catalytic reduction of NO by NH_3. *J. Colloid Interface Sci.* **2022**, *622*, 1–10. [CrossRef] [PubMed]
107. Yin, C.; Hou, C.; Yang, S.; Mao, D.; Liu, J. Research progress in transition metals modified Cu-SSZ-13 zeolite denitration catalyst. *Chem. Ind. Eng. Prog.* **2023**, *42*, 2963–2974.
108. Chen, M.; Li, J.; Xue, W.; Wang, S.; Han, J.; Wei, Y.; Mei, D.; Li, Y.; Yu, J. Unveiling Secondary-Ion-Promoted Catalytic Properties of Cu-SSZ-13 Zeolites for Selective Catalytic Reduction of NO_x. *J. Am. Chem. Soc.* **2022**, *144*, 12816–12824. [CrossRef]
109. Wang, J.; Zhang, J.; Tang, X.; Liu, J.; Ju, M. Research progress on modification of Cu-SSZ-13 catalyst for denitration of automobile exhaust gas. *Chem. Ind. Eng. Prog.* **2023**, *42*, 4636–4648.
110. Chen, Z.; Liu, Q.; Guo, L.; Zhang, S.; Pang, L.; Guo, Y.; Li, T. The promoting mechanism of in situ Zr doping on the hydrothermal stability of Fe-SSZ-13 catalyst for NH_3-SCR reaction. *Appl. Catal. B Environ.* **2021**, *286*, 119816. [CrossRef]
111. Liu, M.; Zhang, G.; Chang, L.; Bao, W.; Wang, J. Study on denitrification performance of titanium doped Cu-SSZ-13 prepared by in-situ method. *Mod. Chem. Ind.* **2019**, *39*, 89–94.
112. Xu, R.; Wang, Z.; Liu, N.; Dai, C.; Zhang, J.; Chen, B.-H. Understanding Zn Functions on Hydrothermal Stability in a One-Pot-Synthesized Cu&Zn-SSZ-13 Catalyst for NH_3 Selective Catalytic Reduction. *ACS Catal.* **2020**, *10*, 6197–6212.
113. Zhao, Z.; Yu, R.; Shi, C.; Gies, H.; Xiao, F.-S.; De Vos, D.; Yokoi, T.; Bao, X.; Kolb, U.; Mcguire, R.; et al. Rare-earth ion exchanged Cu-SSZ-13 zeolite from organotemplate-free synthesis with enhanced hydrothermal stability in NH_3-SCR of NO_x. *Catal. Sci. Technol.* **2019**, *9*, 241–251. [CrossRef]
114. Zhang, T.; Li, J.; Liu, J.; Wang, D.; Zhao, Z.; Cheng, K.; Li, J. High activity and wide temperature window of Fe-Cu-SSZ-13 in the selective catalytic reduction of NO with ammonia. *AIChE J.* **2015**, *61*, 3825–3837. [CrossRef]

115. Wan, J.; Chen, J.; Zhao, R.; Zhou, R. One-pot synthesis of Fe/Cu-SSZ-13 catalyst and its highly efficient performance for the selective catalytic reduction of nitrogen oxide with ammonia. *J. Environ. Sci.* **2021**, *100*, 306–316. [CrossRef] [PubMed]
116. Ming, Y.; Li, G. One-pot synthesis of FeCu–SSZ-13 using Cu–TEPA as the template by adding iron complexes. *Catal. Sci. Technol.* **2021**, *11*, 7467–7474. [CrossRef]
117. Wang, J.; Liu, J.; Tang, X.; Xing, C.; Jin, T. The promotion effect of niobium on the low-temperature activity of Al-rich Cu-SSZ-13 for selective catalytic reduction of NO_x with NH_3. *Chem. Eng. J.* **2021**, *418*, 129433. [CrossRef]
118. Liu, J.; Tang, X.; Xing, C.; Jin, T.; Yin, Y.; Wang, J. Niobium modification for improving the high-temperature performance of Cu-SSZ-13 in selective catalytic reduction of NO by NH_3. *J. Solid State Chem.* **2021**, *296*, 122028. [CrossRef]
119. Usman, M.; Ghanem, A.S.; Niaz Ali Shah, S.; Garba, M.D.; Yusuf Khan, M.; Khan, S.; Humayun, M.; Laeeq Khan, A. A Review on SAPO-34 Zeolite Materials for CO_2 Capture and Conversion. *Chem. Rec.* **2022**, *22*, e202200039. [CrossRef]
120. Wang, L.; Li, W.; Qi, G.; Weng, D. Location and nature of Cu species in Cu/SAPO-34 for selective catalytic reduction of NO with NH_3. *J. Catal.* **2012**, *289*, 21–29. [CrossRef]
121. Huang, S.; Wang, J.; Wang, J.; Wang, C.; Shen, M.; Li, W. The influence of crystallite size on the structural stability of Cu/SAPO-34 catalysts. *Appl. Catal. B Environ.* **2019**, *248*, 430–440. [CrossRef]
122. Wang, A.; Chen, Y.; Walter, E.D.; Washton, N.M.; Mei, D.; Varga, T.; Wang, Y.; Szanyi, J.; Wang, Y.; Peden, C.H.F.; et al. Unraveling the mysterious failure of Cu/SAPO-34 selective catalytic reduction catalysts. *Nat. Commun.* **2019**, *10*, 1137. [CrossRef]
123. Andonova, S.; Tamm, S.; Montreuil, C.; Lambert, C.; Olsson, L. The effect of iron loading and hydrothermal aging on one-pot synthesized Fe/SAPO-34 for ammonia SCR. *Appl. Catal. B Environ.* **2016**, *180*, 775–787. [CrossRef]
124. Wang, D.; Zhang, L.; Kamasamudram, K.; Epling, W.S. In Situ-DRIFTS Study of Selective Catalytic Reduction of NOx by NH3 over Cu-Exchanged SAPO-34. *ACS Catal.* **2013**, *3*, 871–881. [CrossRef]
125. Zhang, S.; Chen, J.; Meng, Y.; Pang, L.; Guo, Y.; Luo, Z.; Fang, Y.; Dong, Y.; Cai, W.; Li, T. Insight into solid-state ion-exchanged Cu-based zeolite (SSZ-13, SAPO-18, and SAPO-34) catalysts for the NH_3-SCR reaction: The promoting role of NH_4-form zeolite substrates. *Appl. Surf. Sci.* **2022**, *571*, 151328. [CrossRef]
126. Tang, J.; Xu, M.; Yu, T.; Ma, H.; Shen, M.; Wang, J. Catalytic deactivation mechanism research over Cu/SAPO-34 catalysts for NH_3-SCR (II): The impact of copper loading. *Chem. Eng. Sci.* **2017**, *168*, 414–422. [CrossRef]
127. Wang, J.-C.; Chen, Y.; Tang, L.; Bao, W.-R.; Chang, L.-P.; Han, L.-N. One-step hydrothermal synthesis of Cu-SAPO-34/cordierite and its catalytic performance on NO_x removal from diesel vehicles. *Trans. Nonferrous Met. Soc. China* **2013**, *23*, 3330–3336. [CrossRef]
128. Zhao, H.; Li, H.; Li, X.; Liu, M.; Li, Y. The promotion effect of Fe to Cu-SAPO-34 for selective catalytic reduction of NO_x with NH_3. *Catal. Today* **2017**, *297*, 84–91. [CrossRef]
129. Doan, T.; Dam, P.; Nguyen, K.; Vuong, T.H.; Le, M.T.; Pham, T.H. Copper-Iron Bimetal Ion-Exchanged SAPO-34 for NH_3-SCR of NO_x. *Catalysts* **2020**, *10*, 321. [CrossRef]
130. Wang, C.; Xu, Q.; Wang, L.; Zhan, W.; Guo, Y.; Guo, Y. Effect of Metal Modification on NH_3-SCR Reaction Performance of Cu-SAPO-34 Catalyst. *Rare Met.* **2020**, *44*, 159–165.
131. Mao, J.-W.; Xu, B.; Hu, Y.-K.; Zhang, C.-Y.; Meng, H.-M. Effect of Ce metal modification on the hydrothermal stability of Cu-SAPO-34 catalyst. *J. Fuel Chem. Technol.* **2020**, *48*, 1208–1216. [CrossRef]
132. Chen, B.; Cheng, J.; Qiao, J.; Dai, C.; Xu, R.; Yu, G.; Wang, N.; Xing, J.; Liu, N. Understanding of low- and high-temperature $DeNO_x$ efficiency for NH_3-SCR via comparison on Cu modified CHA and AFX zeolites. *Fuel* **2023**, *348*, 128501. [CrossRef]
133. Li, R.; Jiang, X.; Lin, J.; Zhang, Z.; Huang, Q.; Fu, G.; Zhu, Y.; Jiang, J. Understanding the influence of hydrothermal treatment on NH_3-SCR of NO activity over Cu-SSZ-16. *Chem. Eng. J.* **2022**, *441*, 136021. [CrossRef]
134. Wei, X.; Ke, Q.; Cheng, H.; Guo, Y.; Yuan, Z.; Zhao, S.; Sun, T.; Wang, S. Seed-assisted synthesis of Cu-(Mn)-UZM-9 zeolite as excellent NO removal and N_2O inhibition catalysts in wider temperature window. *Chem. Eng. J.* **2020**, *391*, 123491. [CrossRef]
135. Fu, G.; Yang, R.; Liang, Y.; Yi, X.; Li, R.; Yan, N.; Zheng, A.; Yu, L.; Yang, X.; Jiang, J. Enhanced hydrothermal stability of Cu/SSZ-39 with increasing Cu contents, and the mechanism of selective catalytic reduction of NO. *Microporous Mesoporous Mater.* **2021**, *320*, 111060. [CrossRef]
136. Du, J.; Han, S.; Huang, C.; Shan, Y.; Zhang, Y.; Shan, W.; He, H. Comparison of precursors for the synthesis of Cu-SSZ-39 zeolite catalysts for NH_3-SCR reaction. *Appl. Catal. B Environ.* **2023**, *338*, 123072. [CrossRef]
137. Han, S.; Tang, X.; Wang, L.; Ma, Y.; Chen, W.; Wu, Q.; Zhang, L.; Zhu, Q.; Meng, X.; Zheng, A.; et al. Potassium-directed sustainable synthesis of new high silica small-pore zeolite with KFI structure (ZJM-7) as an efficient catalyst for NH_3-SCR reaction. *Appl. Catal. B Environ.* **2021**, *281*, 119480. [CrossRef]
138. Bai, Y.; Hao, D.; Wei, Y.; Han, J.; Li, D.; Chen, M.; Yu, J. Copper-exchanged SUZ-4 zeolite catalysts for selective catalytic reduction of NO_x. *Mater. Chem. Front.* **2024**, *8*, 2142–2148. [CrossRef]
139. Ryu, T.; Ahn, N.H.; Seo, S.; Cho, J.; Kim, H.; Jo, D.; Park, G.T.; Kim, P.S.; Kim, C.H.; Bruce, E.L.; et al. Fully Copper-Exchanged High-Silica LTA Zeolites as Unrivaled Hydrothermally Stable NH_3-SCR Catalysts. *Angew. Chem.* **2017**, *129*, 3304–3308. [CrossRef]

140. Zhu, J.; Liu, Z.; Xu, L.; Ohnishi, T.; Yanaba, Y.; Ogura, M.; Wakihara, T.; Okubo, T. Understanding the high hydrothermal stability and NH_3-SCR activity of the fast-synthesized ERI zeolite. *J. Catal.* **2020**, *391*, 346–356. [CrossRef]
141. Martín, N.; Vennestrøm, P.N.R.; Thøgersen, J.R.; Moliner, M.; Corma, A. Iron-Containing SSZ-39 (AEI) Zeolite: An Active and Stable High-Temperature NH_3-SCR Catalyst. *ChemCatChem* **2017**, *9*, 1754–1757. [CrossRef]
142. Tan, X.; Zhang, S.; Hong, S.B. Facile one-pot synthesis of Fe-UZM-35 catalysts for ammonia selective catalytic reduction. *Appl. Catal. B Environ.* **2023**, *329*, 122552. [CrossRef]
143. Grzybek, J.; Gil, B.; Roth, W.J.; Skoczek, M.; Kowalczyk, A.; Chmielarz, L. Characterization of Co and Fe-MCM-56 catalysts for NH_3-SCR and N_2O decomposition: An in situ FTIR study. *Spectrochim. Acta A Mol. Biomol. Spectrosc.* **2018**, *196*, 281–288. [CrossRef]
144. Ming, S.; Chen, Z.; Fan, C.; Pang, L.; Guo, W.; Albert, K.B.; Liu, P.; Li, T. The effect of copper loading and silicon content on catalytic activity and hydrothermal stability of Cu-SAPO-18 catalyst for NH_3-SCR. *Appl. Catal. A-Gen.* **2018**, *559*, 47–56. [CrossRef]
145. Han, S.; Cheng, J.; Ye, Q.; Cheng, S.; Kang, T.; Dai, H. Ce doping to Cu-SAPO-18: Enhanced catalytic performance for the NH_3-SCR of NO in simulated diesel exhaust. *Microporous Mesoporous Mater.* **2019**, *276*, 133–146. [CrossRef]
146. Xin, Y.; Wang, X.; Li, Q.; Ma, X.; Qi, Y.; Zheng, L.; Anderson, J.A.; Zhang, Z. The Potential of Cu-SAPO-44 in the Selective Catalytic Reduction of NO_x with NH_3. *ChemCatChem* **2016**, *8*, 3740–3745. [CrossRef]
147. Zhang, Y.; Peng, Y.; Wang, C.; Li, K.; Liu, S.; Li, X.; Chen, J.; Li, J. Selective Catalytic Reduction of NO_x with Ammonia over Copper Ion Exchanged SAPO-47 Zeolites in a Wide Temperature Range. *ChemCatChem* **2018**, *10*, 2481–2487. [CrossRef]
148. Zhang, S.; Ming, S.; Guo, L.; Bian, C.; Meng, Y.; Liu, Q.; Dong, Y.; Bi, J.; Li, D.; Wu, Q.; et al. Controlled synthesis of Cu-based SAPO-18/34 intergrowth zeolites for selective catalytic reduction of NO_x by ammonia. *J. Hazard. Mater.* **2021**, *414*, 125543. [CrossRef]
149. Gao, Q.; Han, S.; Ye, Q.; Cheng, S.; Kang, T.; Dai, H. Effects of Lanthanide Doping on the Catalytic Activity and Hydrothermal Stability of Cu-SAPO-18 for the Catalytic Removal of NO_x (NH_3-SCR) from Diesel Engines. *Catalysts* **2020**, *10*, 336. [CrossRef]
150. Lin, J.; Hu, X.; Tan, X.; Lin, C.; Zhang, Y.; Shan, W.; He, H. Y-Doped Cu-SSZ-39 Zeolite with Only Cu^{2+}-2Z Species: An NH_3-SCR Catalyst with Extremely High Hydrothermal Stability. *Environ. Sci. Technol.* **2025**, *59*, 15515–15525. [CrossRef]
151. He, S.; Lin, Z.; Shi, J.; Zhou, L.; Cui, Q.; Li, T.; Liu, J.; Yue, Y. Interface-engineered ZnO/FeCu-SSZ-13 with robust SO_2 and H_2O resistance for low-temperature NH_3-SCR. *Chem. Eng. J.* **2025**, *522*, 167119. [CrossRef]
152. Feng, Y.; Janssens, T.V.W.; Vennestrøm, P.N.R.; Jansson, J.; Skoglundh, M.; Grönbeck, H. High-Temperature Reaction Mechanism of NH_3-SCR over Cu-CHA: One or Two Copper Ions? *J. Phys. Chem. C* **2024**, *128*, 6689–6701. [CrossRef]
153. Han, J.; Li, J.; Zhao, W.; Li, L.; Chen, M.; Ge, X.; Wang, S.; Liu, Q.; Mei, D.; Yu, J. Cu-OFF/ERI Zeolite: Intergrowth Structure Synergistically Boosting Selective Catalytic Reduction of NOx with NH_3. *J. Am. Chem. Soc.* **2024**, *146*, 7605–7615. [CrossRef] [PubMed]
154. Bae, S.Y.; Shin, J.S.; Kim, Y.; Lee, J.M. Decision tree analysis on the performance of zeolite-based SCR catalysts. *IFAC-Pap.* **2021**, *54*, 55–60. [CrossRef]
155. Meng, X.; Xiao, F.S. Green routes for synthesis of zeolites. *Chem. Rev.* **2014**, *114*, 1521–1543. [CrossRef]
156. Nanda, A.S.F.; Kadja, G.T.M. Bio-based templates for generating hierarchical zeolites: An overview for greener synthesis pathway. *J. Porous Mater.* **2024**, *31*, 1155–1173. [CrossRef]
157. Pan, T.; Wu, Z.; Yip, A.C.K. Advances in the Green Synthesis of Microporous and Hierarchical Zeolites: A Short Review. *Catalysts* **2019**, *9*, 274. [CrossRef]
158. Ren, L.; Zhu, L.; Yang, C.; Chen, Y.; Sun, Q.; Zhang, H.; Li, C.; Nawaz, F.; Meng, X.; Xiao, F.S. Designed copper–amine complex as an efficient template for one-pot synthesis of Cu-SSZ-13 zeolite with excellent activity for selective catalytic reduction of NOx by NH_3. *Chem. Commun.* **2011**, *47*, 9789–9791. [CrossRef]
159. Li, Q.; Cong, W.; Zhang, J.; Xu, C.; Wang, F.; Han, D.; Wang, G.; Bing, L. Rapid synthesis of hierarchical nanosized SSZ-13 zeolite with excellent MTO catalytic performance. *Microporous Mesoporous Mater.* **2022**, *331*, 111649. [CrossRef]
160. Miao, M.; Qiu, Y.; Yao, L.; Wu, Q.; Ruan, H.; Van Der Bruggen, B.; Shen, J. Preparation of *N,N,N*-trimethyl-1-adamantylammonium hydroxide with high purity via bipolar membrane electrodialysis. *Sep. Purif. Technol.* **2018**, *205*, 241–250. [CrossRef]
161. Xiong, W.; Liu, L.; Guo, A.; Chen, D.; Shan, Y.; Fu, M.; Wu, J.; Ye, D.; Chen, P. Economical and Sustainable Synthesis of Small-Pore Chabazite Catalysts for NOx Abatement by Recycling Organic Structure-Directing Agents. *Environ. Sci. Technol.* **2023**, *57*, 655–665. [CrossRef]
162. Debost, M.; Clatworthy, E.B.; Grand, J.; Barrier, N.; Nesterenko, N.; Gilson, J.-P.; Boullay, P.; Mintova, S. Direct synthesis of nanosized CHA zeolite free of organic template by a combination of cations as structure directing agents. *Microporous Mesoporous Mater.* **2023**, *358*, 112337. [CrossRef]

163. Hrabanek, P.; Zikanova, A.; Supinkova, T.; Drahokoupil, J.; Fila, V.; Lhotka, M.; Dragounova, H.; Laufek, F.; Brabec, L.; Jirka, I.; et al. Static in-situ hydrothermal synthesis of small pore zeolite SSZ-16 (AFX) using heated and pre-aged synthesis mixtures. *Microporous Mesoporous Mater.* **2016**, *228*, 107–115. [CrossRef]
164. Bossche, A.V.D.; Rodriguez, N.R.; Riaño, S.; Dehaen, W.; Binnemans, K. Dissolution behavior of precious metals and selective palladium leaching from spent automotive catalysts by trihalide ionic liquids. *RSC Adv.* **2021**, *11*, 10110–10120. [CrossRef] [PubMed]

Disclaimer/Publisher's Note: The statements, opinions and data contained in all publications are solely those of the individual author(s) and contributor(s) and not of MDPI and/or the editor(s). MDPI and/or the editor(s) disclaim responsibility for any injury to people or property resulting from any ideas, methods, instructions or products referred to in the content.